

High Signal-to-Noise Echelle Spectroscopy of QSO Absorption Line Systems with Metals in the Direction of HS 1700+6416¹

Todd M. Tripp^{2,3}, Limin Lu^{4,5}, and Blair D. Savage²

ABSTRACT

We have obtained a high signal-to-noise ($30 \leq S/N \leq 70$) high resolution (FWHM = 20 km s^{-1}) spectrum of the radio-quiet QSO HS 1700+6416 ($z_{\text{em}} = 2.72$) with the echelle spectrograph on the KPNO 4m telescope. We detect 13 metal systems in the optical spectrum of this QSO, including six systems with associated optically thin Lyman limit absorption in the *HST* spectrum obtained by Reimers et al. We use the apparent column density technique and profile fitting to measure the heavy element column densities and to evaluate the impact of unresolved absorption saturation. Profile fitting indicates that four of the C IV systems are narrow with $b < 8 \text{ km s}^{-1}$, which implies that these absorbers are relatively cool and probably photoionized.

The dense cluster of C IV doublets at $2.432 < z_{\text{abs}} < 2.441$ shows the weak line of one C IV absorber apparently aligned with the strong line of a different C IV doublet, i.e., line locked, for two pairs of C IV absorbers. Line locking has been detected previously in $z_{\text{abs}} \approx z_{\text{em}}$ absorbers where radiation pressure is likely to play a role, but it is surprising in this case since this C IV complex is displaced by $\sim 24000 \text{ km s}^{-1}$ from the QSO emission redshift. This may be the remnant (or precursor) of a broad absorption line (BAL) outflow. However, it is possible that these alignments are chance alignments rather than true line locking.

The high ion column density ratios in the multicomponent Lyman limit absorber at $z_{\text{abs}} = 2.3150$ suggest that the ionization conditions in this absorber differ significantly from the conditions in the gaseous halo of the Milky Way. From photoionization models we derive $[\text{Si}/\text{H}] \geq -0.95$ and $[\text{Al}/\text{H}] \geq -0.96$ for the strongest component of this absorber. These are conservative lower limits derived from lower ionization stages only; photoionization models in agreement with the observed low and high ionization

¹Based on observations obtained with the Kitt Peak National Observatory 4 m telescope, which is operated by the Association of Universities for Research in Astronomy (AURA) under contract with the National Science Foundation.

²Department of Astronomy, University of Wisconsin - Madison, 475 N. Charter St., Madison, WI 53706 - 1582, Electronic mail: tripp@astro.princeton.edu, savage@madraf.astro.wisc.edu

³Current address: Princeton University Observatory, Peyton Hall, Princeton, NJ 08544

⁴Astronomy Department, 105-24, California Institute of Technology, Pasadena, CA 91125, Electronic mail: ll@astro.caltech.edu

⁵Hubble Fellow

stages require $[M/H] \approx -0.45$. In contrast, Vogel & Reimers derive $[N/H] < -1.04$ and $[O/H] = -1.52$ for this absorber. We suggest that the discrepancy is due to the low resolution of the Vogel & Reimers data ($\text{FWHM} \approx 300 \text{ km s}^{-1}$) which introduces serious blending and saturation problems. The photoionized model with $[M/H] = -0.45$ has a particle density $n_H \approx 0.02 \text{ cm}^{-3}$, a size of a few hundred pc, and a mass of roughly $1 \times 10^5 M_\odot$, assuming the absorber is spherical.

We detect unsaturated C IV and rather strong N V “associated” absorption at $z_{\text{abs}} = 2.7125$. The apparent column density of the weak N V 1242.8 Å line is greater than the apparent column density of the stronger N V 1238.8 Å line in this absorber, which indicates that the N V profile is affected by unresolved saturation or that the N V absorbing gas does not completely cover the QSO emission source. If the latter interpretation is correct, then the associated absorbing gas must be close to the QSO. We have used the observed spectral energy distribution of the QSO, corrected for intervening Lyman limit absorption, for photoionization modeling of the associated absorber, and we derive $[N/H] \geq -0.65$ and $[C/H] \geq -0.82$. Other corrections (e.g., to account for dust in intervening absorbers or ‘Lyman valley’ attenuation) will make the spectral energy distribution harder and increase the metallicity estimates. However, the absorption profiles suggest that the constant density single slab model is too simplistic: we obtain $b(\text{N V}) = 25.2 \pm 1.3 \text{ km s}^{-1}$ and $b(\text{C IV}) = 11.4 \pm 1.1 \text{ km s}^{-1}$ from profile fitting, and therefore the gas which produces the N V absorption does not have the same temperature and non-thermal motions as the C IV gas.

Finally, we briefly examine the number of Mg II systems detected per unit redshift, and we tentatively conclude that dN/dz is dominated by weak Mg II lines with $W_r < 0.3 \text{ \AA}$.

Subject headings: galaxies: ISM — quasars: absorption lines — quasars: individual (HS 1700+6416)

1. Introduction

The successful deployment of the *Hubble Space Telescope* (*HST*) has opened many windows for the study of the high redshift universe. In the spectroscopic arena, the *HST* Faint Object Spectrograph (FOS) observation of the luminous radio-quiet QSO HS 1700+6416 ($z_{\text{em}} = 2.72$) by Reimers et al. (1992) has provided an extraordinary spectrum which demonstrates the potential of the *HST* for the study of high z QSO absorption lines. This FOS spectrum has yielded results on topics about which little or nothing was known before the launch of the *HST*, including (1) the helium content of QSO absorbers at $z_{\text{abs}} > 1.84$, and (2) an ultra-highly ionized phase of QSO absorbers traced by species such as Ne VIII (see also Hamann et al. 1995), which may reveal the presence of gas with $T \gg 10^5 \text{ K}$ (Verner, Tytler, & Barthel 1994). These new topics

are observationally challenging because the resonance lines of He I, He II, and the ultra-highly ionized species (e.g., Ne VIII, Mg X, and Si XII) all occur at rest wavelengths $\lambda_r < 912 \text{ \AA}$, and only a handful of QSOs are currently known with continuum flux detected at $\lambda_r \ll 912 \text{ \AA}$ (c.f. Beaver et al. 1991; Jakobsen et al. 1994; §6.1 in Tripp, Bechtold, & Green 1994; Reimers et al. 1995b; Lyons et al. 1995; Tytler et al. 1995). The continua of background QSOs with sufficient redshift to show these absorption lines are usually undetectable due to attenuation by intervening absorption, either optically thick Lyman limit (LL) absorption or the cumulative effect of many absorbers along the line of sight (c.f., Møller & Jakobsen 1990; Picard & Jakobsen 1993). The HS 1700+6416 sight line has its share of LL absorbers — seven LL systems are well-detected in the Reimers et al. FOS spectrum — but remarkably all of the LLs are optically thin ($\tau_{\text{LL}} \lesssim 1$) and the quasar continuum is detected from ~ 1200 to 3250 \AA , which corresponds to ~ 320 to 870 \AA in the QSO restframe.

In addition to the ground-breaking *HST* spectrum, this sight line is intriguing because a deep ROSAT PSPC image obtained by Reimers et al. (1995a) shows two extended X-ray sources within a few arcminutes of the QSO. Both of these X-ray objects are flagged as greater than 3σ extended sources by the SHARC survey (see Romer et al. 1996a, 1996b). One of these X-ray sources is Abell 2246, a galaxy cluster at $z = 0.225$. The other extended source is less easily identified and may be a higher redshift galaxy cluster. The close proximity of these X-ray objects to the sight line offers the tantalizing possibility of studying the detailed properties of galaxy intracluster media detected in absorption in the spectrum of HS 1700+6416.

HS 1700+6416 is also an excellent target for ground-based studies of LL absorbers. Since the LL systems in the *HST* spectrum are all optically thin, the Lyman continuum optical depth can be measured, and this provides an accurate estimate of the H I column density. Previous studies of LL absorbers (e.g., Steidel 1990) have mostly used samples of optically thick LL systems and have been forced to rely on elaborate methods to estimate $N(\text{H I})$. To study the abundances and physical conditions in LL systems, and to complement space-based programs, we have obtained a high resolution (FWHM = 20 km s^{-1}) high signal-to-noise optical spectrum of HS 1700+6416, and in this paper we present the data and analyses of the absorption systems. The paper is organized as follows. We briefly review the observations and data reduction in §2 and the line selection and column density measurements in §3. In §4 we provide some comments on the individual absorption systems including assessments of absorption line saturation. In this section we also comment on a dense cluster of C IV absorbers at $2.432 < z_{\text{abs}} < 2.441$ in which the weak lines of some C IV absorbers are well-aligned with the strong lines of different C IV doublets. In §5 we discuss the physical conditions and abundances in the absorption systems. In §6 we examine the number of Mg II absorbers detected per unit redshift including weak absorbers. After some comments on the abundances derived by Vogel & Reimers (1995) from the low resolution FOS spectrum in §7, we summarize the paper in §8.

2. Observations and Data Reduction

The observations and data reduction techniques are fully described in Tripp et al. (1996); we summarize a few of the pertinent details here. HS 1700+6416 was observed during darktime (18–20 May 1993) with the echelle spectrograph and the T2KB 2048×2048 CCD on the 4m telescope at Kitt Peak National Observatory (KPNO). With a $1''.33 \times 9''.7$ entrance aperture, the instrument setup provided a resolution of 20 km s^{-1} with ~ 2 pixels/FWHM and spectral coverage from 4300 to 8350 Å with no gaps between echelle orders. Five one-hour observations were obtained over the course of three nights.

The preliminary data reduction (overscan and bias subtraction, flatfielding, etc.) was done with IRAF following the standard procedure. The “optimal” spectrum extraction routine described by Horne (1986; see also Robertson 1986) was used to extract the final spectra from the individual observations, and then the individual spectra were rebinned to the same wavelength scale and coadded. In addition to the flux spectrum, the optimal extraction program yields a 1σ error spectrum which includes the contribution from read noise as well as statistical noise, and this error spectrum was propagated throughout the data reduction and analysis procedures. The coadded spectrum was normalized by fitting cubic splines to regions free of absorption lines. Overlapping regions of adjacent orders were weighted by their signal-to-noise ratios and coadded. The final normalized spectrum of HS 1700+6416 is shown in Figure 1. The signal-to-noise ratio of the final spectrum ranges from ~ 30 to 70 per resolution element at $\lambda > 4550 \text{ Å}$ (the S/N is somewhat lower within the Ly α forest).

3. Data Analysis

3.1. Absorption Line Selection and Identification

Absorption lines in the HS 1700+6416 spectrum were selected for analysis based on the statistical significance of the observed equivalent width W_λ . Absorption line equivalent widths were measured using the automated method described in Tripp et al. (1996). Telluric absorption

Fig. 1.— (following pages) Normalized spectrum of HS 1700+6416 obtained with the echelle spectrograph on the KPNO 4m telescope, plotted as a function of vacuum heliocentric wavelength. Absorption lines due to extragalactic metals are marked with a number that identifies the line in column 1 of Table 1. At $\lambda < 4560 \text{ Å}$, most of the absorption lines are due to the Ly α forest. The resolution is 20 km s^{-1} with $30 \lesssim S/N \lesssim 70$ per resolution element (the S/N decreases somewhat below 4500 Å). The zero level is indicated with a dashed line, and the solid line near zero is the 1σ uncertainty due to photon statistics and read noise. The discontinuous increase in the flux uncertainty at $\lambda \approx 4520 \text{ Å}$ is due to a bad column in the CCD which prevented coaddition of overlapping orders. Telluric absorption lines have not been removed from this spectrum.

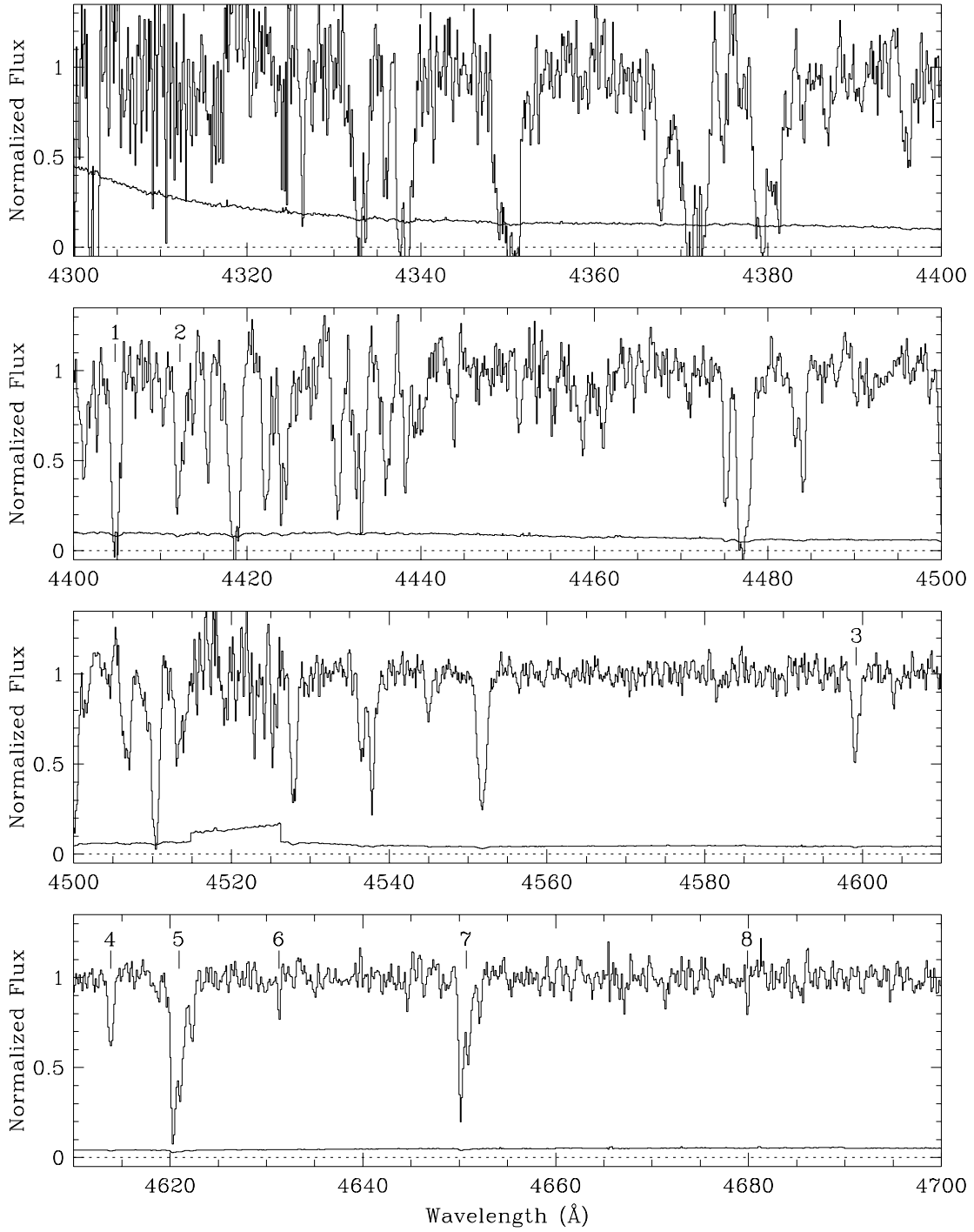


Fig. 1.— continued

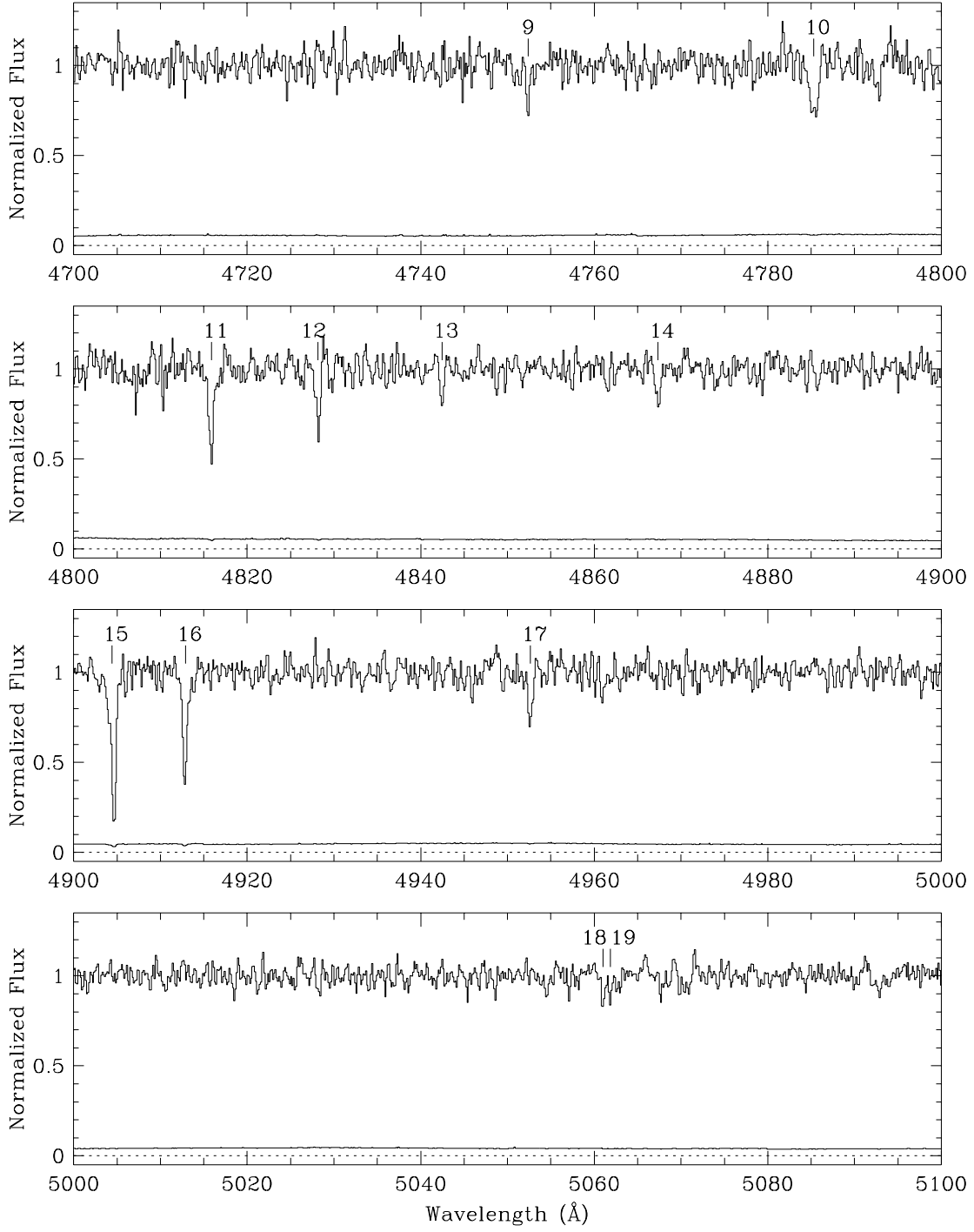


Fig. 1.— continued

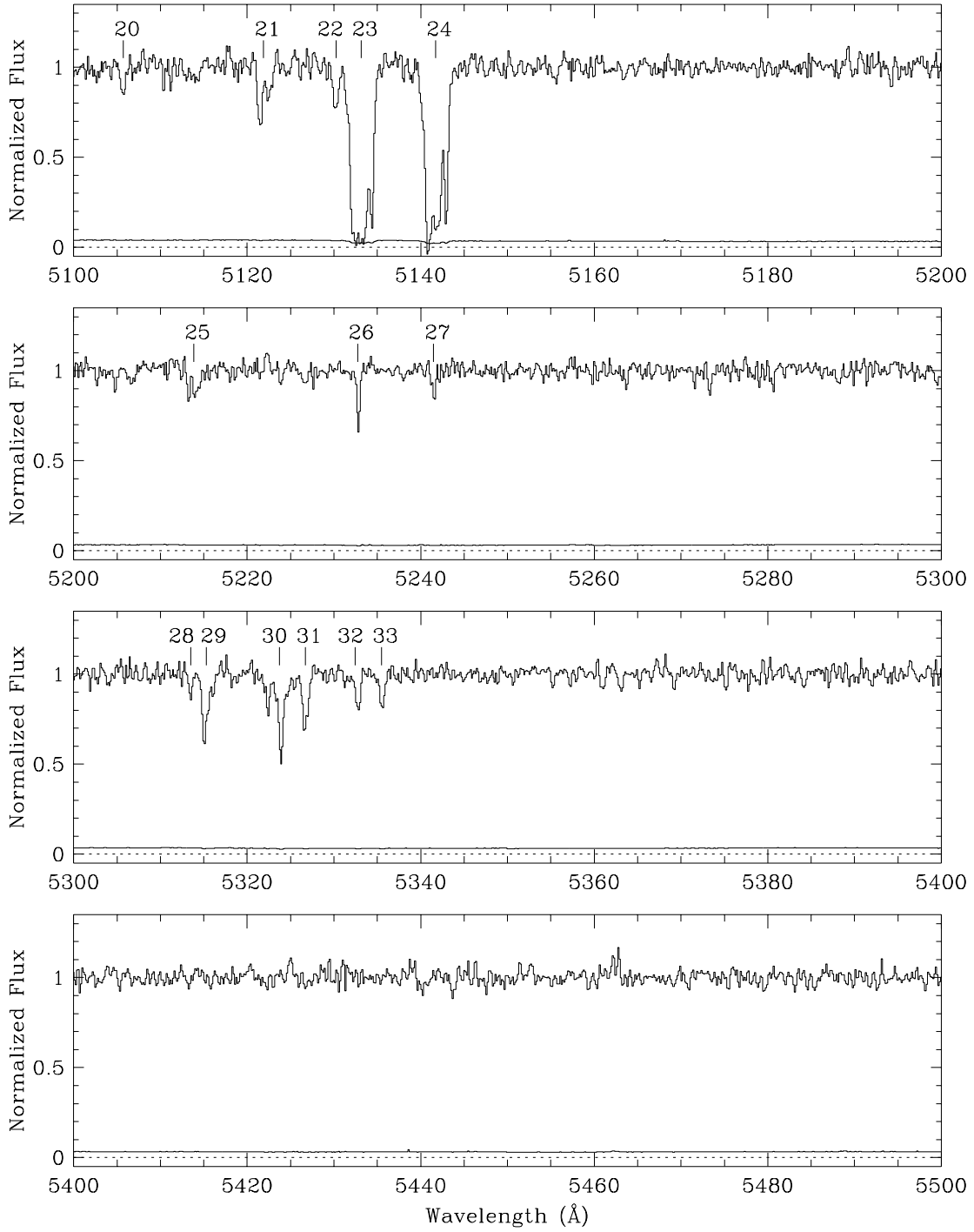


Fig. 1.— continued

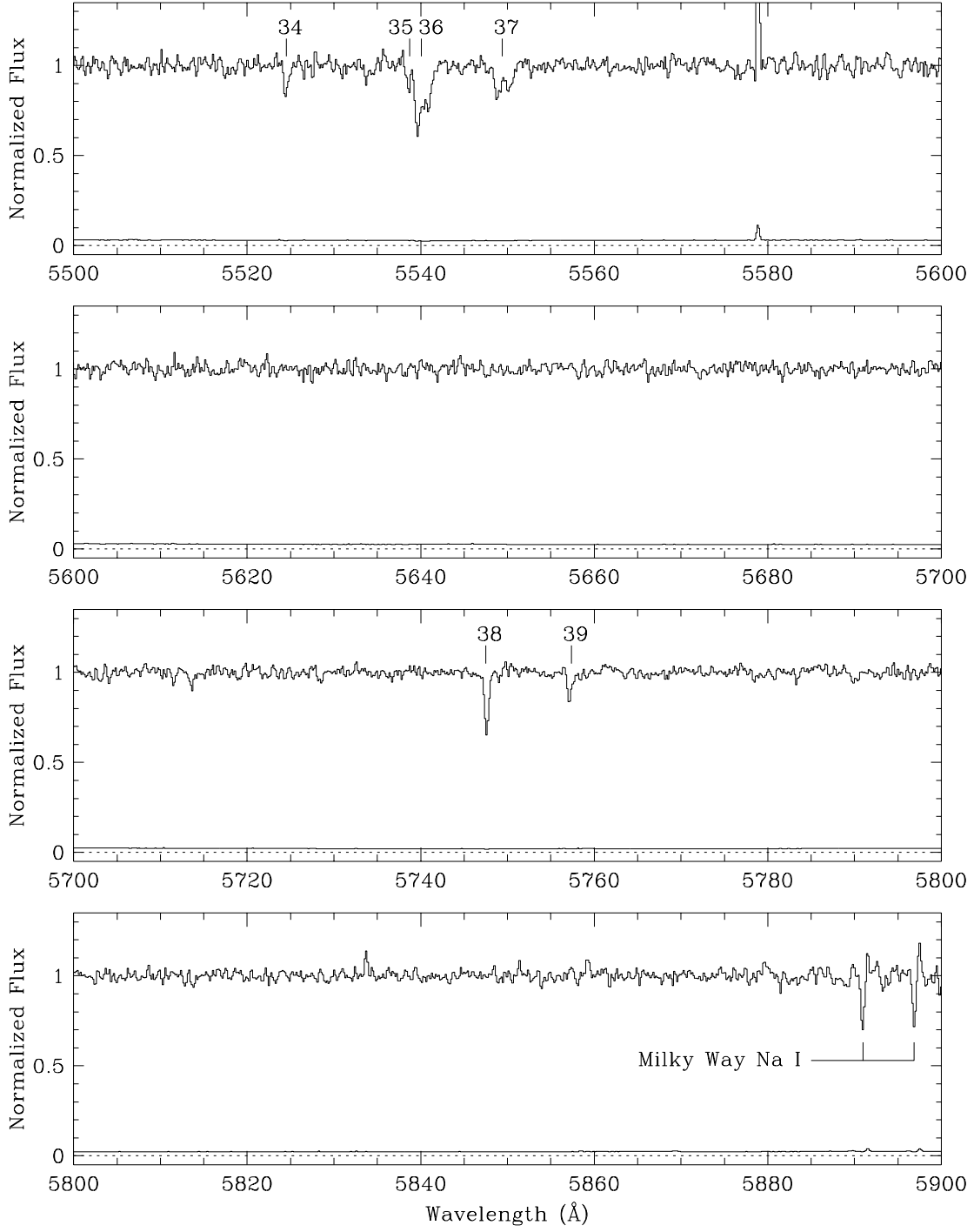


Fig. 1.— continued

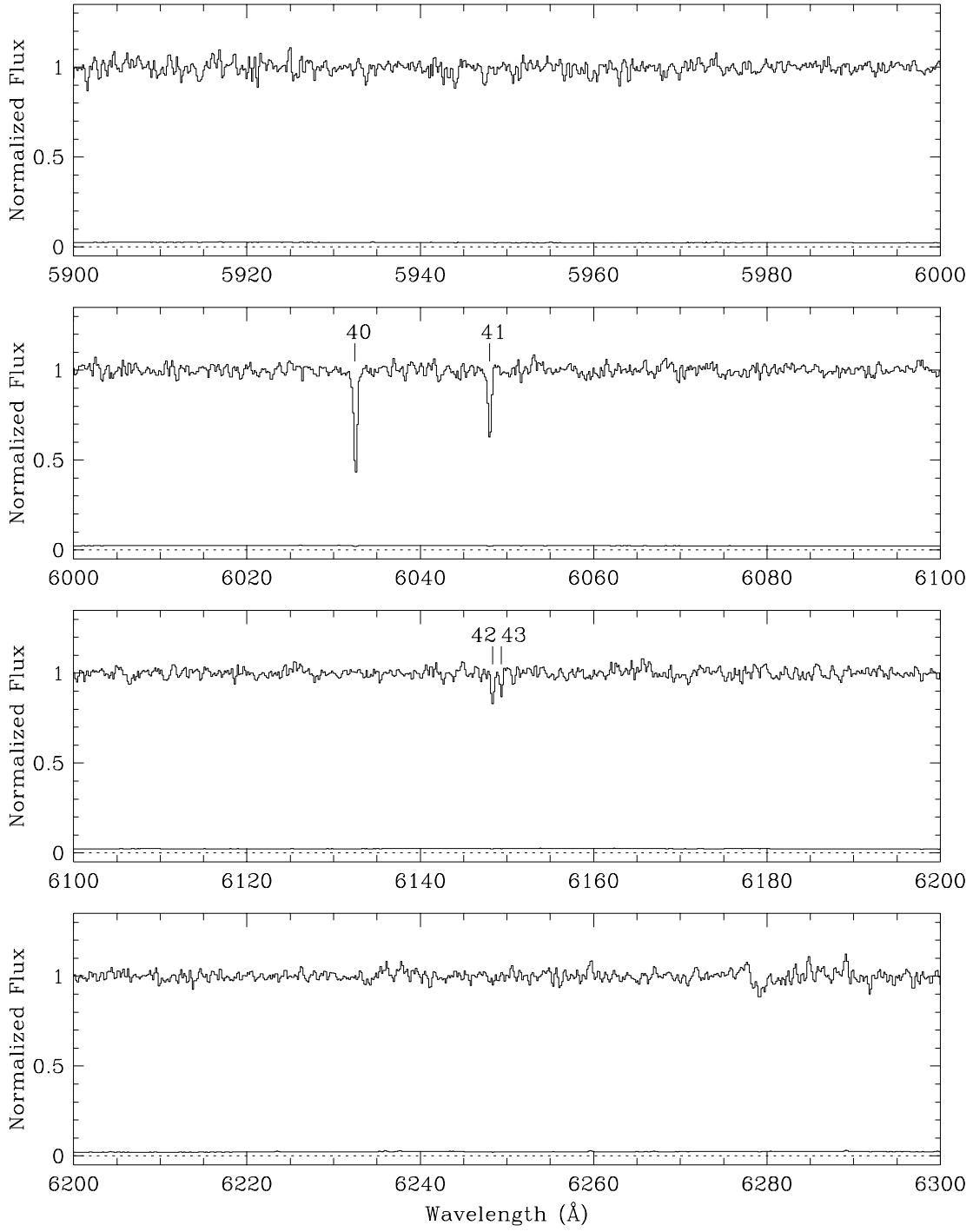


Fig. 1.— continued

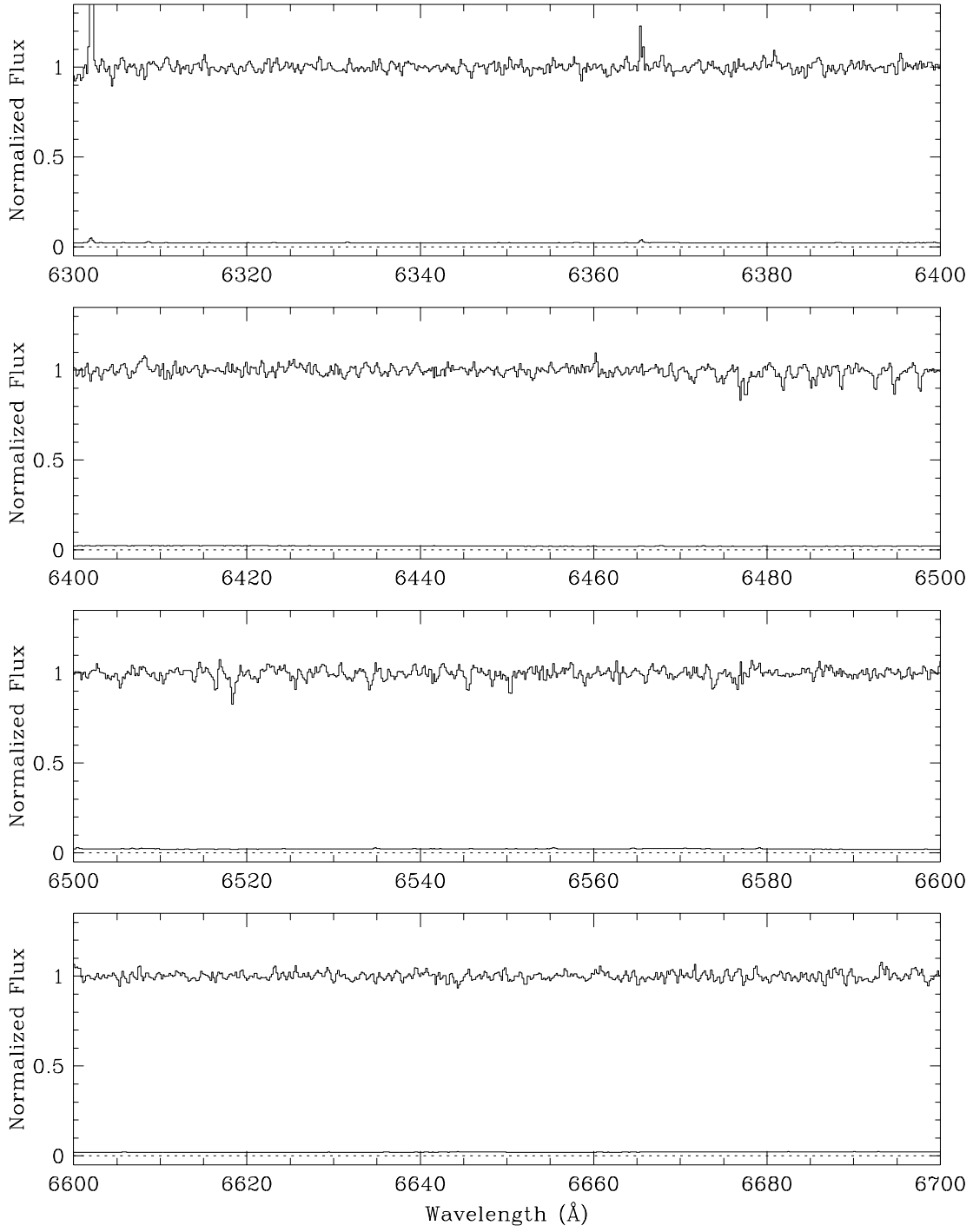


Fig. 1.— continued

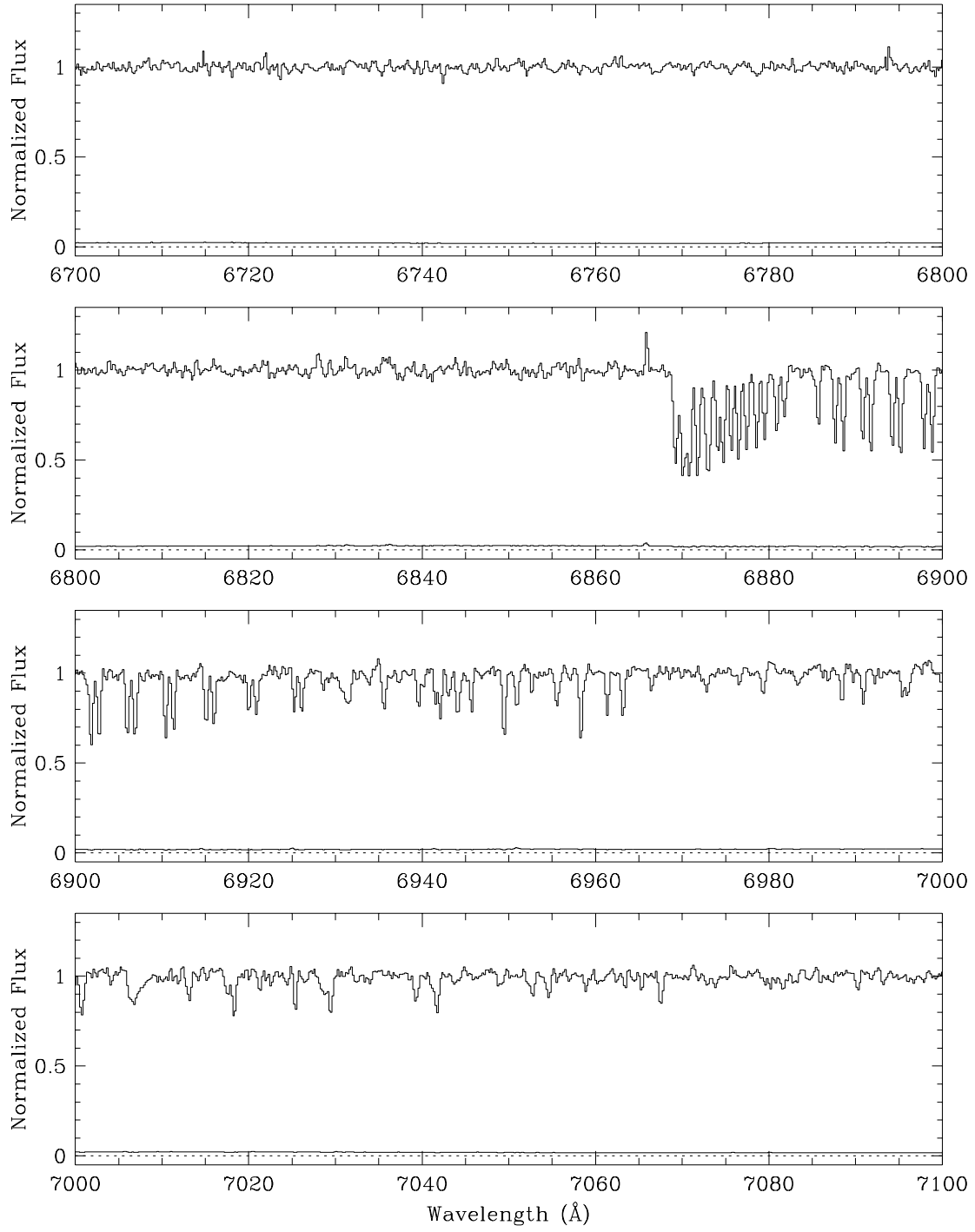


Fig. 1.— continued

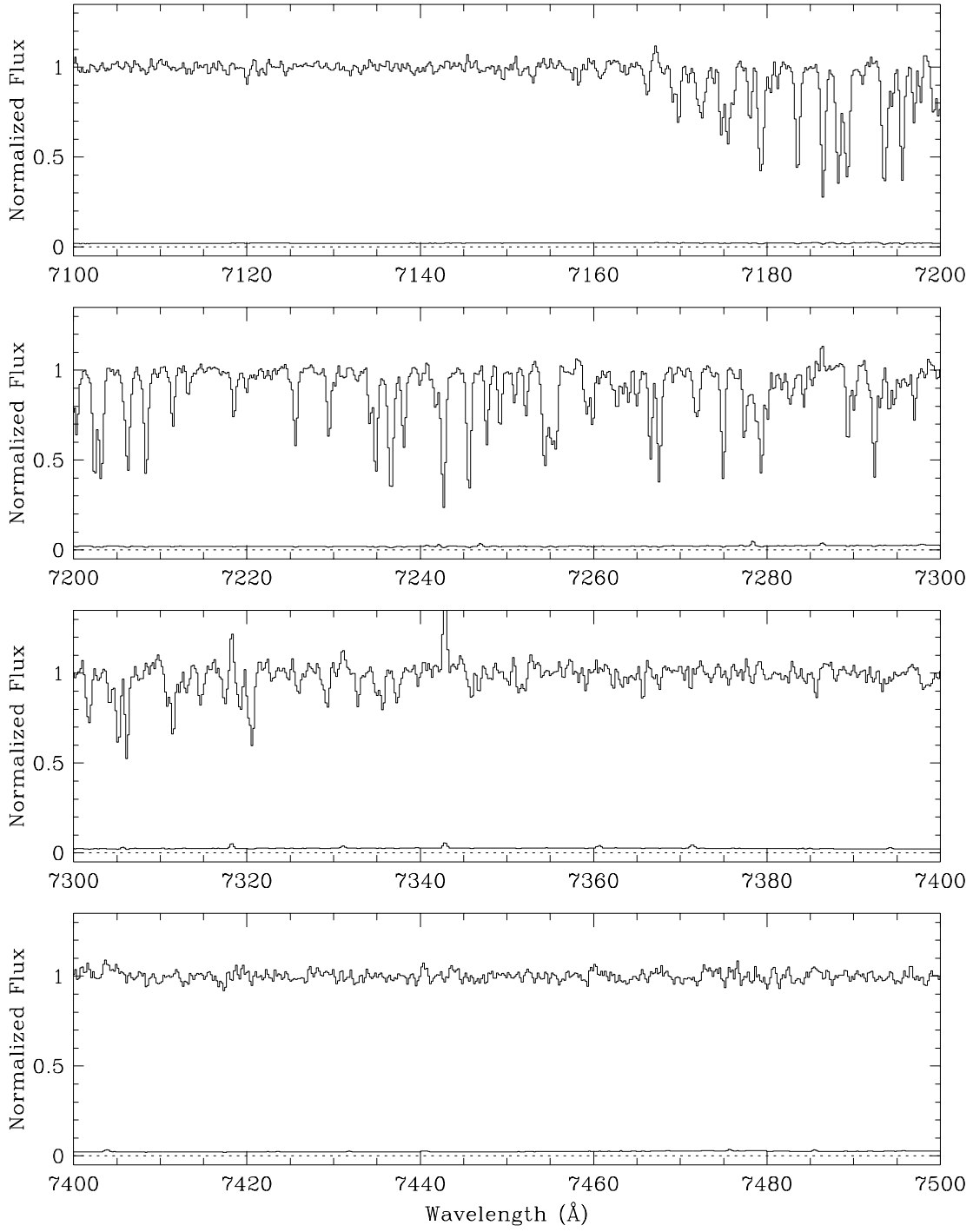


Fig. 1.— continued

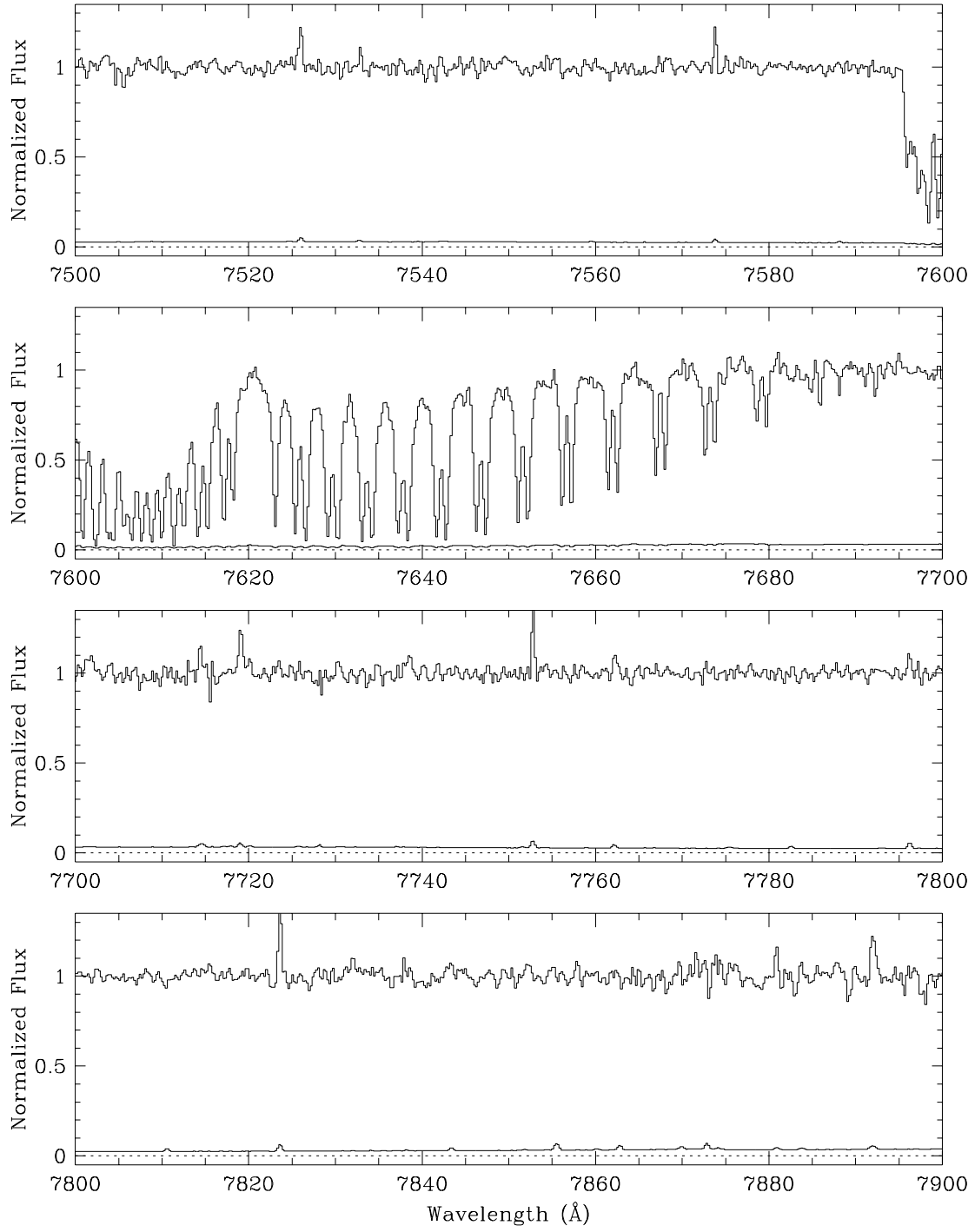


Fig. 1.— continued

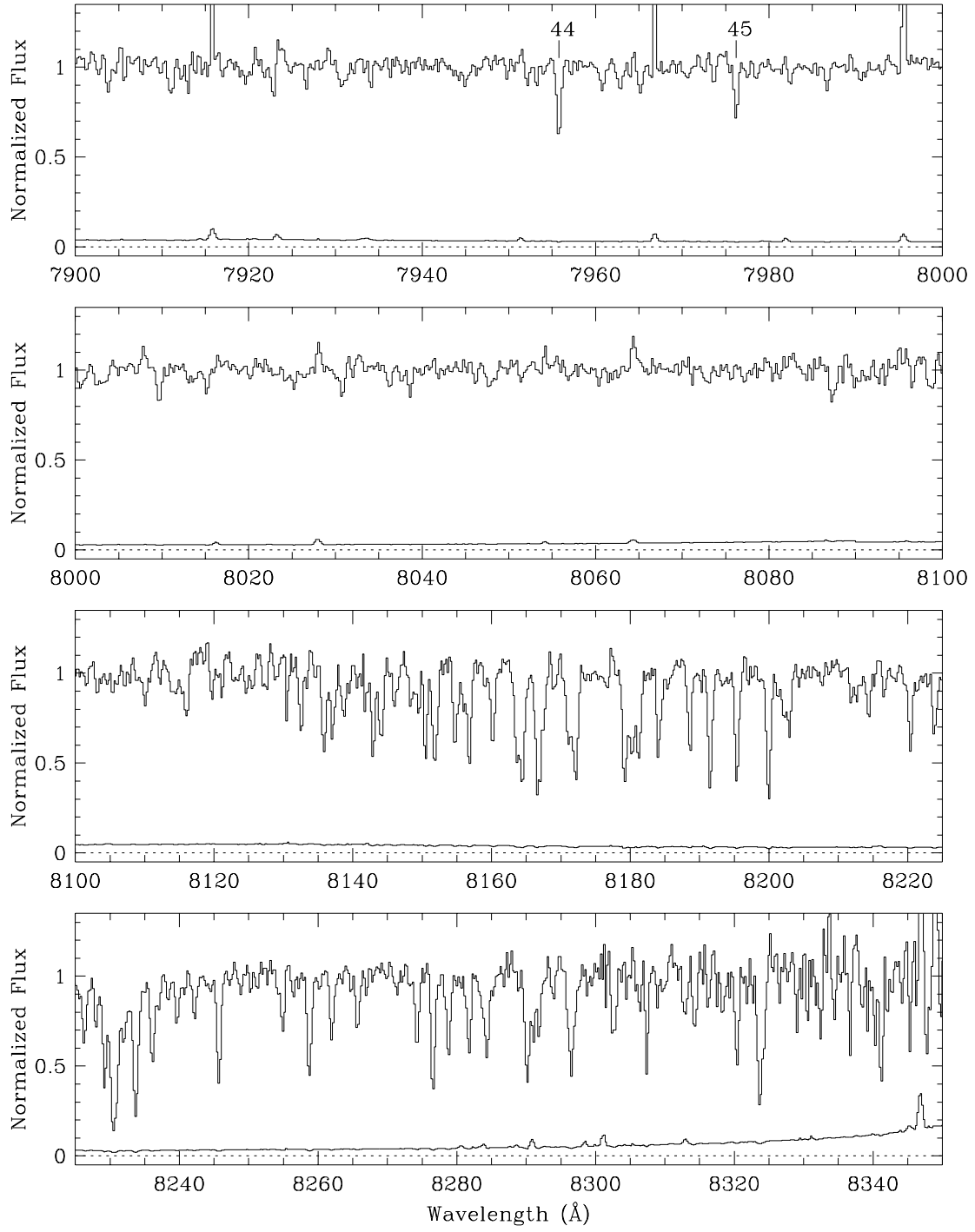


Fig. 1.— continued

lines were removed from the line list by comparing the normalized spectrum of HS 1700+6416 to the normalized spectrum of HS 1946+7658 obtained during the same observing run. Since the HS 1700+6416 and HS 1946+7658 spectra have similar S/N levels and the same resolution, atmospheric absorption lines are effectively removed in a ratio of the two spectra (see Figure 3 in Tripp et al. 1996). We have used this ratio of the HS 1700+6416 spectrum to the HS 1946+7658 spectrum to identify telluric lines *only*; for all other measurements reported in this paper we use the coadded spectrum shown in Figure 1 (which has not been divided by the HS 1946+7658 spectrum).

Table 1 lists all statistically significant ($W_\lambda \geq 4\sigma$) extragalactic absorption lines detected in the KPNO HS 1700+6416 spectrum. Table 1 also lists the heliocentric vacuum wavelength of the centroid of each absorption line and a line number which identifies the absorption line in Figure 1. Identifications of the line species derived from the Morton (1991) finding list are tabulated in column 4 of Table 1, and Table 2 summarizes by redshift the heavy element systems we detect in the spectrum of this quasar. We have detected 13 heavy element absorbers in the direction of this quasar, 6 of which also produce detectable Lyman limits in the FOS spectrum of HS 1700+6416 obtained by Reimers et al. (1992). There are several absorption features in Table 1 for which we could not find positive identifications (labeled “UID” in column 4 of Table 1). Most of these unidentified lines are weak ($< 5\sigma$), so they could be the C IV 1548.2 Å line with the corresponding C IV 1550.8 Å line falling below our detection threshold. Similarly, some of these UIDs could be the stronger line in the Mg II doublet with the weaker line undetected.

Table 1. Heavy Element Absorption Lines in the Optical Spectrum of HS 1700+6416^a

Line Number	λ_{vac} (Å)	$W_{\lambda} \pm \sigma_W$ (Å)	Identification	z_{abs}	$\log N$ (cm ⁻²)	b (km s ⁻¹)	$\log N_{\text{a}}$ (cm ⁻²)
(1)	(2)	(3)	(4)	(5)	(6)	(7)	(8)
1	4404.79	1.175±0.070	C IV 1548.2 ^b	1.84515	14.35±0.03	32.6±1.6	>14.32
2	4412.26	0.843±0.059	C IV 1550.8 ^b	1.84515	14.35±0.03	32.6±1.6	14.33±0.04
3	4599.17	0.457±0.043	N V 1238.8	2.71248	13.86±0.02	25.2±1.3	13.78±0.03
4	4613.85	0.253±0.028	N V 1242.8	2.71248	13.86±0.02	25.2±1.3	13.87±0.04
5	4620.93	1.322±0.043	Si IV 1393.8	2.31457	12.05±0.14	5.0±16.5	12.06±0.14
				2.31499	13.75±0.07	10.4±1.1	13.60±0.03
				2.31550	13.52±0.03	30.9±2.4	13.41±0.02
				2.31642	12.92±0.03	13.8±2.0	12.89±0.04
6	4631.32	0.066±0.014	UID
7	4650.72	0.848±0.051	Si IV 1402.8	2.31457	12.05±0.14	5.0±16.5	...
				2.31499	13.75±0.07	10.4±1.1	13.68±0.03
				2.31550	13.52±0.03	30.9±2.4	13.40±0.04
				2.31642	12.92±0.03	13.8±2.0	12.89±0.10
8	4679.89	0.057±0.013	UID
9	4752.37	0.113±0.026	UID
10	4785.28	0.303±0.052	Si IV 1393.8	2.43339	13.05±0.04	32.7±4.6	13.05±0.08
11	4815.90	0.370±0.046	Mg II 2796.4	0.72219	12.78±0.03	16.2±1.7	12.74±0.05
12	4828.16	0.202±0.030	Mg II 2803.5	0.72219	12.78±0.03	16.2±1.7	12.80±0.08
13	4842.45	0.094±0.020	UID
14	4867.35	0.125±0.029	UID
15	4904.41	0.702±0.055	C IV 1548.2	2.16797	13.94±0.02	16.5±0.8	13.90±0.02
16	4912.92	0.456±0.046	C IV 1550.8	2.16797	13.94±0.02	16.5±0.8	13.94±0.04
17	4952.66	0.162±0.024	UID
18	5061.03	0.087±0.023	Si II 1526.7	2.31499	13.08±0.07*	9.4±5.2	13.07±0.12
19	5061.87	0.052±0.014	Si II 1526.7	2.31553	12.86±0.20
20	5105.72	0.098±0.025	UID

Table 1—Continued

Line Number	λ_{vac} (Å)	$W_{\lambda} \pm \sigma_W$ (Å)	Identification	z_{abs}	$\log N$ (cm^{-2})	b (km s^{-1})	$\log N_{\text{a}}$ (cm^{-2})
(1)	(2)	(3)	(4)	(5)	(6)	(7)	(8)
21	5121.89	0.333±0.036	C IV 1548.2 ^d	2.30812	13.38±0.03	25.0±2.2	...
			UID
22	5130.23	0.181±0.023	C IV 1550.8 ^d	2.30812	13.38±0.03	25.0±2.2	...
23	5133.14	2.672±0.031	C IV 1548.2	2.31458	13.19±0.11	14.6±5.4	} >14.74 ^c
				2.31505	15.48±1.1	11.3±3.8	
				2.31568	14.57±0.02	28.6±1.5	
				2.31638	16.72±0.14	3.9±0.2	
24	5141.71	2.477±0.039	C IV 1550.2	2.31458	13.19±0.11	14.6±5.4	} >14.93 ^c
				2.31505	15.48±1.1	11.3±3.8	
				2.31568	14.57±0.02	28.6±1.5	
				2.31638	16.72±0.14	3.9±0.2	
25	5213.84	0.177±0.027	Mg II 2796.4 ^e	0.86431	12.00±0.05	6.0±4.8	...
			UID
26	5232.72	0.156±0.030	C IV 1548.2	2.37995	13.13±0.04	6.3±2.0	13.07±0.06
27	5241.48	0.075±0.014	C IV 1550.8	2.37995	13.13±0.04	6.3±2.0	13.03±0.15
28	5313.49	0.060±0.019	C IV 1548.2	2.43204	12.70±0.07	8.0±5.5	12.66±0.17
29	5315.29	0.332±0.036	C IV 1548.2	2.43306	13.16±0.19	4.0±3.5	} 13.44±0.05 ^c
				2.43329	13.29±0.05	44.5±4.9	
30	5323.70	0.578±0.056	C IV 1548.2 ^f	2.43785	12.80±0.06	12.6±4.3	...
				2.43877	13.30±0.03	18.3±1.9	...
			C IV 1550.8	2.43204	12.70±0.07	8.0±5.5	...
				2.43306	13.16±0.19	4.0±3.5	...
				2.43329	13.29±0.05	44.5±4.9	...
31	5326.70	0.233±0.025	C IV 1548.2	2.44059	13.30±0.02	20.3±1.7	13.28±0.05
32	5332.45	0.167±0.032	C IV 1550.8	2.43785	12.80±0.06	12.6±4.3	12.70 ^{+0.20} _{-0.37}
				2.43877	13.30±0.03	18.3±1.9	13.35±0.10
33	5335.48	0.136±0.028	C IV 1550.8	2.44059	13.30±0.02	20.3±1.7	13.28±0.10
34	5524.54	0.105±0.018	UID
35	5538.74	0.060±0.019	Al II 1670.8	2.31498	11.71±0.06*	7.9±4.6	11.69±0.11
36	5540.05	0.552±0.035	C IV 1548.2	2.57813	13.34±0.03	18.9±1.9	} 16.64±0.03 ^c
				2.57884	13.36±0.03	35.0±3.8	
37	5549.41	0.311±0.043	C IV 1550.8	2.57813	13.34±0.03	18.9±1.9	} 16.63±0.06 ^c
				2.57884	13.36±0.03	35.0±3.8	

Table 1—Continued

Line Number	λ_{vac} (Å)	$W_{\lambda} \pm \sigma_W$ (Å)	Identification	z_{abs}	$\log N$ (cm ⁻²)	b (km s ⁻¹)	$\log N_a$ (cm ⁻²)
(1)	(2)	(3)	(4)	(5)	(6)	(7)	(8)
38	5747.49	0.218±0.027	C IV 1548.2	2.71245	13.19±0.02	11.4±1.1	13.18±0.04
39	5757.38	0.120±0.021	C IV 1550.8	2.71245	13.19±0.02	11.4±1.1	13.16±0.08
40	6032.45	0.330±0.027	Mg II 2796.4	1.15729	12.80±0.03	6.7±0.6	12.65±0.03
41	6047.98	0.192±0.014	Mg II 2803.5	1.15729	12.80±0.03	6.7±0.6	12.67±0.05
42	6148.36	0.069±0.012	Al III 1854.7	2.31499	12.20±0.18*	3.2±5.8	12.11±0.09
43	6149.34	0.045±0.010	Al III 1854.7	2.31551	11.95±0.18*	2.8±9.0	11.87±0.18
44	7955.79	0.222±0.019	Mg II 2796.4	1.84506	12.65±0.10	3.5±0.7	12.31±0.06
45	7976.21	0.142±0.015	Mg II 2803.5	1.84506	12.65±0.10	3.5±0.7	12.43±0.08

^aNOTES: The line number in column 1 identifies the absorption feature in Figure 1. Column 2 lists the vacuum heliocentric wavelength of the absorption feature, and column 3 gives the observed equivalent width. Column 4 identifies the species and lists the vacuum rest wavelength of the line; in this column “UID” indicates that the line is unidentified. Columns 5, 6, and 7 give the absorption redshift, logarithmic column density, and Doppler parameter, respectively, determined from profile fitting, and column 8 lists the logarithm of the integrated apparent column density (see §3.2). Most of the column densities and Doppler parameters from profile fitting are based on the simultaneous fitting of more than one absorption line for the ion (e.g., simultaneous fitting of C IV 1548.2 and C IV 1550.8 Å). Profile fitting column densities which are based on fitting of a *single* line are marked with an asterisk in column 6.

^bThese metal lines are found in the Ly α forest and thus could be contaminated by H I absorption from different redshifts (see §4.5).

^cThe various components of this absorption feature are blended with adjacent components, and column (8) lists the total column density integrated across all components.

^dThese lines are detected at high significance levels, but the line identifications are tentative (see §4.7), and due to significant blending with unidentified absorption, integrated column densities are not reliable.

^eThis absorption feature is confused by blending with unidentified absorption, and the Mg II identification is not secure (see §4.2).

^fDue to very strong blending of the C IV 1548.2 and 1550.8 Å lines in this absorption feature (see Figure 4), the integrated apparent column densities are not useful (the apparent optical depth of the 1548.2 Å line cannot be distinguished from the $\tau_a(v)$ of the 1550.8 Å line).

3.2. Column Densities

Column densities of identified absorption lines were measured using two techniques, the apparent column density method and profile fitting. Once again, these measurements are discussed in some detail in Tripp et al. (1996).

In the apparent column density method, the “apparent” (i.e., observed) optical depth per unit velocity, $\tau_a(v)$, is used to calculate the apparent column density as a function of velocity according to the following relation:

$$N_a(v) = \frac{m_e c}{\pi e^2} \left(\frac{\tau_a(v)}{f \lambda} \right) = 3.768 \times 10^{14} \left(\frac{\tau_a(v)}{f \lambda} \right) \quad (\text{atoms cm}^{-2} (\text{km s}^{-1})^{-1}), \quad (1)$$

where f is the oscillator strength and λ is the wavelength of the transition (in Å), and the other symbols have their usual meanings. The apparent optical depth is determined from the observed normalized absorption line profile, $I(v)$, according to the usual relation, $\tau_a(v) = \ln[1/I(v)]$. If the line profile is fully resolved, then $N_a(v)$ provides a good estimate of the true column density per unit velocity. Even if the profile is not well-resolved, $N_a(v)$ still provides a good representation of the true column density, broadened by the spectral spread function, *if* the profile is not affected by unresolved saturation. However, if the profile contains unresolved saturated absorption, then $N_a(v)$ will be an underestimate of the true column density. If two or more resonance lines of a species differing in the quantity $f\lambda$ are available, then comparison of the $N_a(v)$ profiles of the different lines can be used to search for unresolved saturation. If the absorption profile contains unresolved saturated components, then the $N_a(v)$ of stronger lines will be less than the $N_a(v)$ of weaker lines at velocities where the saturation occurs. If there is no unresolved saturation, the resonance lines will yield the same $N_a(v)$. Finally, if the absorption profile is not affected by unresolved saturated components, then $N_a(v)$ can be integrated to obtain a good measurement of the total column density, $N(\text{total}) = N_a = \int N_a(v) dv$. The error in $N_a(v)$ due to uncertainty of the continuum placement is estimated as described in Tripp et al. (1996), and this error is added in quadrature to the error from photon counting and read noise to get the total uncertainty in $N_a(v)$. Integrated apparent column densities of all metals detected in the HS 1700+6416 spectrum are given in column 8 of Table 1. For further information on the apparent column density method, see Savage & Sembach (1991), Jenkins (1996), and references therein. For most of the lines in Table 1 we use oscillator strengths and wavelengths from Morton (1991). However, for some transitions we use the oscillator strength revisions summarized in Tripp et al. (1996).

We have also used the profile fitting routine described by Lanzetta & Bowen (1992) to estimate column densities by fitting Voigt profiles to the HS 1700+6416 absorption lines, and we refer the reader to their paper for a description of the minimized χ^2 profile fitting procedure. For the purposes of this paper, we have fitted different lines from the same ion (e.g., C IV 1548.2 Å and C IV 1550.8 Å) simultaneously, but we have fitted different elements and different ionization stages independently. The column densities, Doppler parameters, and redshifts obtained by fitting Voigt profiles in this fashion are listed in columns 5, 6, and 7 of Table 1. Voigt profile fitting

corrects for saturated absorption to some degree,⁶ but direct integration of $N_a(v)$ does not correct for saturation effects unless special efforts are made (Savage & Sembach 1991; Jenkins 1996). Therefore for a specific line, comparison of the column density derived from profile fitting to the column density given by direct integration of $N_a(v)$ can also be used to assess the impact of unresolved saturated absorption. If the column density from profile fitting is significantly larger than the integrated apparent column density, then the absorption line may be affected by unresolved saturation.

4. Comments on Individual Systems

In the HS 1700+6416 discovery paper, Reimers et al. (1989) identified four metal absorption systems at $z_{\text{abs}} = 2.308, 2.315, 2.433,$ and 2.440 on the basis of C IV lines detected in a high resolution but modest S/N optical spectrum. Subsequently, Reimers et al. (1992) reobserved the quasar with the *HST* FOS and detected a wide range of ionization stages of many heavy elements at these redshifts. They also reported detections of metals at $z_{\text{abs}} = 0.8642, 1.1572, 1.725, 1.8465, 2.1678,$ and 2.579 . Reimers et al. (1992) detected H I Lyman continuum absorption in seven of these systems, and all of the Lyman limits have moderate optical depth ($\tau_{LL} \lesssim 1$). This is important because with detection of flux shortward of the Lyman limit edge, the Lyman continuum optical depth $\tau_{LL}(\lambda)$ at wavelength $\lambda \leq 912 \text{ \AA}$ can be reliably measured. Since the cross section for H I continuum absorption is well known, it is then straightforward to estimate the H I column density,

$$N(\text{H I}) = 1.6 \times 10^{17} \tau_{LL}(\lambda) \left[\frac{912}{\lambda} \right]^3. \quad (2)$$

Because of the low resolution of the FOS spectrum, this provides a measurement of the *total* H I column density in the Lyman limit system and no information about the kinematics of the absorber.

More recently, HS 1700+6416 has been observed from the ground by Sanz et al. (1993), Rodríguez-Pascual et al. (1995), and Petitjean, Riediger, & Rauch (1996). Sanz et al. (1993) and Rodríguez-Pascual et al. (1995) have concentrated their efforts on the Ly α forest; they obtained high resolution spectra of the forest and low resolution spectra longward of the Ly α emission line. Petitjean et al. (1995) have observed the quasar longward of Ly α emission but with moderate resolution (FWHM $\sim 95 \text{ km s}^{-1}$).

Table 2 summarizes the heavy element systems we have identified in the KPNO optical spectrum shown in Figure 1. Table 2 also lists the H I column densities determined by Reimers et al. (1992) from τ_{LL} as discussed above. We detect 13 metal systems including new systems at z_{abs}

⁶However, column densities derived from profile fitting can have *large* uncertainties if the line is significantly saturated. These uncertainties may be larger than the errors formally determined in the profile fitting process because the true profile may be more complex than the assumed profile.

Table 2. Summary of Heavy Element Systems

z_{abs}	Species detected	HST LL ^a	$\log N(\text{H I})^{\text{b}}$
0.72219	Mg II 2796.4,2803.5		...
0.86431	Mg II 2796.4,2803.5	✓	16.35
1.15729	Mg II 2796.4,2803.5	✓	16.85
1.725	...	✓	17.05
1.84506	Mg II 2796.4,2803.5	✓	16.75
	C IV 1548.2,1550.8 ^c		
2.16797	C IV 1548.2,1550.8	✓	16.85
2.30812	C IV 1548.2,1550.8		...
2.315,2.316	Si II 1526.7	✓	16.85
	Al II 1670.8		...
	Al III 1854.7,1862.8		...
	Si IV 1393.8,1402.8		...
	C IV 1548.2,1550.8		...
2.37995	C IV 1548.2,1550.8		...
2.433 ^d	Si IV 1393.8	✓	16.7
	C IV 1548.2,1550.8		...
2.439 ^d	C IV 1548.2,1550.8		...
2.44059	C IV 1548.2,1550.8		...
2.57813,2.57884	C IV 1548.2,1550.8		...
2.7125 ^e	C IV 1548.2,1550.8		...
	N V 1238.8,1242.8		...

^aAbsorption systems with associated Lyman continuum absorption in the *HST* spectrum of Reimers et al. (1992) are indicated with a check mark in this column.

^bNeutral hydrogen column density derived by Reimers et al. (1992) from the Lyman continuum optical depth measured in the *HST* FOS spectrum. Reimers et al. do not provide the uncertainties of these $N(\text{H I})$ measurements.

^cThese C IV lines occur in the Ly α forest and could be contaminated by H I from different redshifts.

^dAt least four C IV doublets are detected in a complex absorption cluster at $2.432 < z_{\text{abs}} < 2.441$ (see text §4.10).

^eAssociated absorption system ($z_{\text{abs}} \approx z_{\text{em}}$).

= 2.37995 and 2.44059. In this section we comment on these metal systems including assessments of absorption saturation effects on the column density measurements. Our KPNO spectrum covers the portion of the Ly α forest between $\lambda \approx 4300 \text{ \AA}$ and $\lambda = 4520 \text{ \AA}$, so in principle we can measure the H I column densities of the metal systems at $z_{\text{abs}} = 2.57813$, 2.57884 and $z_{\text{abs}} = 2.7125$ from the Ly α absorption profile. However, the H I lines at 2.57813 and 2.57884 are badly blended and saturated, so the values of $N(\text{H I})$ are not usefully constrained by our spectrum. The highest redshift metal absorber is found at $z_{\text{abs}} = 2.7125$, but there are at least five additional H I Ly α lines at $2.7125 < z_{\text{abs}} \leq 2.74427$ which are not detected in any metal lines despite high S/N in spectral regions where these metal lines would be observed.

4.1. $z_{\text{abs}} = 0.72219$

Reimers et al. (1992) did not recognize this metal system in their initial analysis of the *HST* FOS spectrum, but it was identified in the reanalysis by Vogel & Reimers (1995). Confirmation of this system was provided by Petitjean et al. (1996) who detected the Mg II lines at 2796.4 and 2803.5 \AA . We also detect this Mg II doublet (lines 11 and 12 in Figure 1), and comparison of the apparent column densities of the Mg II lines indicates that there is some unresolved saturation in the core of the Mg II 2796.4 \AA profile. The Mg II 2796.4 \AA line (the stronger member of the doublet) is mildly blended with Si IV 1402.8 \AA absorption from the $z_{\text{abs}} = 2.433$ system; this blending could mask some saturation in the Mg II profile because the excess optical depth from the Si IV line artificially boosts the Mg II 2796.4 \AA $N_{\text{a}}(v)$. However, the weaker Mg II 2803.5 \AA line yields an integrated column density in good agreement with the column density from profile fitting (see Table 1), so this magnesium doublet is only weakly saturated. Reimers et al. (1992) do not report detection of Lyman continuum absorption at this redshift, but the Lyman limit occurs in a region of the FOS spectrum which has very low S/N.

4.2. $z_{\text{abs}} = 0.86431$

This system produces partial Lyman continuum absorption in the *HST* FOS spectrum, and from the Lyman limit optical depth Reimers et al. (1992) estimate that $\log N(\text{H I}) = 16.35$ [unfortunately, Reimers et al. (1992) do not provide the uncertainties in their measurements of $N(\text{H I})$]. We detect a 6.6σ absorption feature (line 25 in Fig. 1) at the expected wavelength of Mg II 2796.4 \AA at this redshift. We consider this to be a probable, but not definite, identification. We detect a 2.3σ absorption line at the expected wavelength (5226.65 \AA) of Mg II 2803.5 \AA , but this weak line does not line up well with the stronger line: the stronger line is best-fit with $z_{\text{abs}} = 0.86452$ while the weaker line indicates that $z_{\text{abs}} = 0.86431$. However, the stronger line shows evidence of two components, and one of the components is reasonably fit with $z_{\text{abs}} = 0.86431$. On this basis, we tentatively conclude that the stronger Mg II line is blended with an unidentified absorption feature. The $N_{\text{a}}(v)$ profiles of these Mg II lines are rather noisy so it is difficult to

assess the impact of unresolved saturation, but these lines are weak and unlikely to be saturated.

4.3. $z_{\text{abs}} = 1.15729$

This metal system produces obvious Lyman continuum absorption in the *HST* spectrum, and Reimers et al. (1992) find that $\log N(\text{H I}) = 16.85$. The Mg II 2796.4 and 2803.5 Å lines at this redshift are recorded at high significance levels in the KPNO spectrum (see lines 40 and 41 in Figure 1 and Table 1). The integrated apparent column densities of these Mg II lines are in agreement, but inspection of the $N_{\text{a}}(v)$ profiles suggests that they are undersampled, and the higher column density from profile fitting indicates that the lines may be moderately affected by unresolved saturation.

4.4. $z_{\text{abs}} = 1.725$

No metals are unambiguously detected in this absorption system, which is identified on the basis of obvious Lyman limit absorption in the *HST* spectrum with $\log N(\text{H I}) = 17.05$ (Reimers et al. 1992). The redshift is not favorable for clear detection of many metal lines from the ground; only the Al II, Al III, Fe II, and Mg II resonance lines are sufficiently redshifted to escape from the Ly α forest. Unfortunately, the Mg II 2796.4, 2803.5 Å doublet at this redshift falls within the O₂ atmospheric A band (see Figure 1), but after removal of the A band using the HS 1946+7658 spectrum as a template (see §3.1), we still do not see any convincing absorption which can be attributed to Mg II. The strongest Fe II line at 2382.8 Å is redshifted into a cleaner region of the optical spectrum; the weak telluric lines near the expected wavelength of this Fe line are effectively removed after division by the template, and the strong Fe II line is not evident after removal of the atmospheric lines. Petitjean et al. (1996) point out that the strong and broad line at 4551.8 Å could be Al II 1670.8 Å at $z_{\text{abs}} = 1.7243$, but this line occurs at the edge of the Ly α forest and Petitjean et al. acknowledge that it could be H I Ly α at $z_{\text{abs}} = 2.744$ instead. We strongly prefer the H I identification for this line because such a strong and broad Al II line⁷ should be accompanied by Mg II absorption which is easily detected (even within the telluric A band), but strong Mg II absorption is not seen. We cannot confidently place upper limits on the column densities of metals we do not detect in this system because the redshift is not adequately constrained by the *HST* spectrum (see §7). The Mg II 2796.4 and 2803.5 Å lines are among the strongest resonance lines typically detected in neutral interstellar gas in the Milky Way (see, for example, §3.4 in Lockman & Savage 1995), so the absence of these lines in absorption suggests that this Lyman limit system is highly ionized.

⁷If the line at 4551.8 Å is indeed Al II 1670.8 Å, then from profile fitting with one component we find $\log N(\text{Al II}) = 13.1$ with $b = 41.9 \text{ km s}^{-1}$.

4.5. $z_{\text{abs}} = 1.84506$

Reimers et al. (1992) and Vogel & Reimers (1995) identify a Lyman limit system at $z_{\text{abs}} = 1.8465$ in the *HST* FOS spectrum of HS 1700+6416, and from the measured τ_{LL} they estimate that $\log N(\text{H I}) = 16.75$. We do not detect any metals at $z_{\text{abs}} = 1.8465$, but we do detect the Mg II 2796.4, 2803.5 Å doublet at $z_{\text{abs}} = 1.84506$ (lines 44 and 45 in Figure 1) at high significance levels. Our KPNO spectrum covers the C IV doublet at this redshift, and two strong absorption features are present at the expected wavelengths of the 1548.2 and 1550.8 Å transitions (see lines 1 and 2 in Figure 1). These C IV lines occur within the Ly α forest and thus are prone to confusion due to blending with H I absorption from different redshifts; however, the velocity extents, centroids, and even the $N_{\text{a}}(v)$ profiles derived from lines 1 and 2 are in reasonable agreement, and we believe these absorption features are primarily due to C IV at this redshift.

Comparison of the Mg II $N_{\text{a}}(v)$ profiles indicates that these magnesium lines are significantly affected by unresolved saturated absorption. Similarly, comparison of the C IV $N_{\text{a}}(v)$ profiles suggests that the C IV column density may be slightly underestimated due to unresolved saturation, but it is important to bear in mind that the C IV column might also be overestimated due to contamination by Ly α forest lines.

4.6. $z_{\text{abs}} = 2.16797$

The C IV 1548.2 and 1550.8 Å lines are clearly detected at this redshift (lines 15 and 16 in Figure 1), and Reimers et al. (1992) report Lyman limit absorption as well with $\log N(\text{H I}) = 16.85$. Inspection of the $N_{\text{a}}(v)$ profiles indicates that these C IV lines are not significantly affected by saturation, and this conclusion is supported by the good agreement of the column densities from profile fitting and $N_{\text{a}}(v)$ integration (see Table 1). Therefore $N(\text{C IV})/N(\text{H I}) = 1.23 \times 10^{-3}$. This column density ratio is similar to the ratio measured in lower $N(\text{H I})$ Ly α clouds by Cowie et al. (1995). However, we report this ratio with some trepidation because the *HST* Lyman limit provides an estimation of the *total* H I column density, and while some of this H I absorption is likely to be associated with the observed C IV lines, there may be additional H I gas which does not produce C IV absorption.

4.7. $z_{\text{abs}} = 2.30812$

Reimers et al. (1992) identified this system based on detection of Lyman series lines as well as various metal lines. At first glance, lines 21 and 22 in Figure 1 appear to be at the expected wavelengths of the C IV 1548.2, 1550.8 Å doublet at this redshift. However, closer inspection of these lines casts some doubt on this identification. First, line 21 shows two components while line 22 shows only one. Line 22 is close to the strong and complex C IV 1548.2 Å absorption

at $z_{\text{abs}} = 2.315$, but it is separated enough to at least partially show two components and the second component is not apparent. The second component of line 21 is not telluric, but it could be an unidentified line from a different redshift. However, line 22 is significantly broader than the stronger component of line 21, and most importantly, lines 21 and 22 do not line up as well: profile fitting gives $z_{\text{abs}} = 2.30805$ for the stronger component of line 21 and $z_{\text{abs}} = 2.30817$ for line 22. We were unable to find a better identification for these lines, so we tentatively suggest that these are the C IV lines, substantially confused by blending, at the redshift of the *HST* system. Line 22 could be an additional component of the multicomponent C IV 1548.2 Å profile at $z_{\text{abs}} = 2.315$, but in this case a corresponding line should be detected in the C IV 1550.8 Å profile at $z_{\text{abs}} = 2.315$, and nothing is apparent at the expected wavelength (see Figure 2).

4.8. $z_{\text{abs}} = 2.3150, 2.3155$

This absorption system, which is detected in Si II, Si IV, C IV, Al II, and Al III, is the most prominent heavy element system in our optical spectrum of HS 1700+6416. This system also shows Lyman limit absorption in the FOS spectrum, and from this Reimers et al. (1992) measure $\log N(\text{H I}) = 16.85$. Figure 2 shows the normalized absorption profiles of all metals we detect in this system (excluding profiles which occur in the Ly α forest). Two components are apparent in the Si II and Al III absorption profiles⁸, and at least three components are clearly present in the profiles of Si IV and C IV. We shall refer to these main components at $z_{\text{abs}} = 2.3150, 2.3155$, and 2.3164 as components 1, 2, and 3 respectively (as labeled in Figure 2). In addition, the C IV 1548.2 and 1550.8 Å profiles both show absorption at $z_{\text{abs}} \approx 2.3146$ (i.e., at $v \approx -40 \text{ km s}^{-1}$ in Figure 2), and very weak absorption is present at this redshift in the Si IV 1393.8 Å profile. There are some indications of further component structure in the profiles (see below), but the combined S/N and resolution of these data do not warrant addition of more components to the profile fits.

Unfortunately, the Al II 1670.8 Å absorption occurs close to the C IV 1548.2 Å absorption line at $z_{\text{abs}} = 2.578$. Furthermore, the $z_{\text{abs}} = 2.578$ absorber shows multiple components ($z_{\text{abs}} = 2.57813$ and $z_{\text{abs}} = 2.57884$), so the identification of the absorption line at 5538.7 Å is ambiguous; this absorption could be due to Al II in component 1 (see Figure 2), or it could be a third component of the C IV absorber at $z_{\text{abs}} = 2.57746$. The C IV 1550.8 Å profile at $z_{\text{abs}} = 2.578$ does not show a third component at $z_{\text{abs}} = 2.57746$, so the line at 5538.7 Å is probably due to Al II. However, we cannot rule out the C IV identification because the line is weak, and it may fall below our detection threshold in the weaker C IV 1550.8 Å profile.

In Figure 3 we compare the apparent column density profiles of the Si IV 1393.8 and 1402.8 Å lines (panel a) as well as the C IV 1548.2 and 1550.8 Å lines (panel b) and the Al III 1854.7 Å

⁸The absorption lines at $z_{\text{abs}} = 2.3150$ and 2.3155 are detected at the 5.7σ and 4.5σ levels, respectively, in the Al III 1854.7 Å transition. Given the weakness of these lines, it is not surprising that they are not significantly detected in the weaker Al III 1862.8 Å line of this doublet.

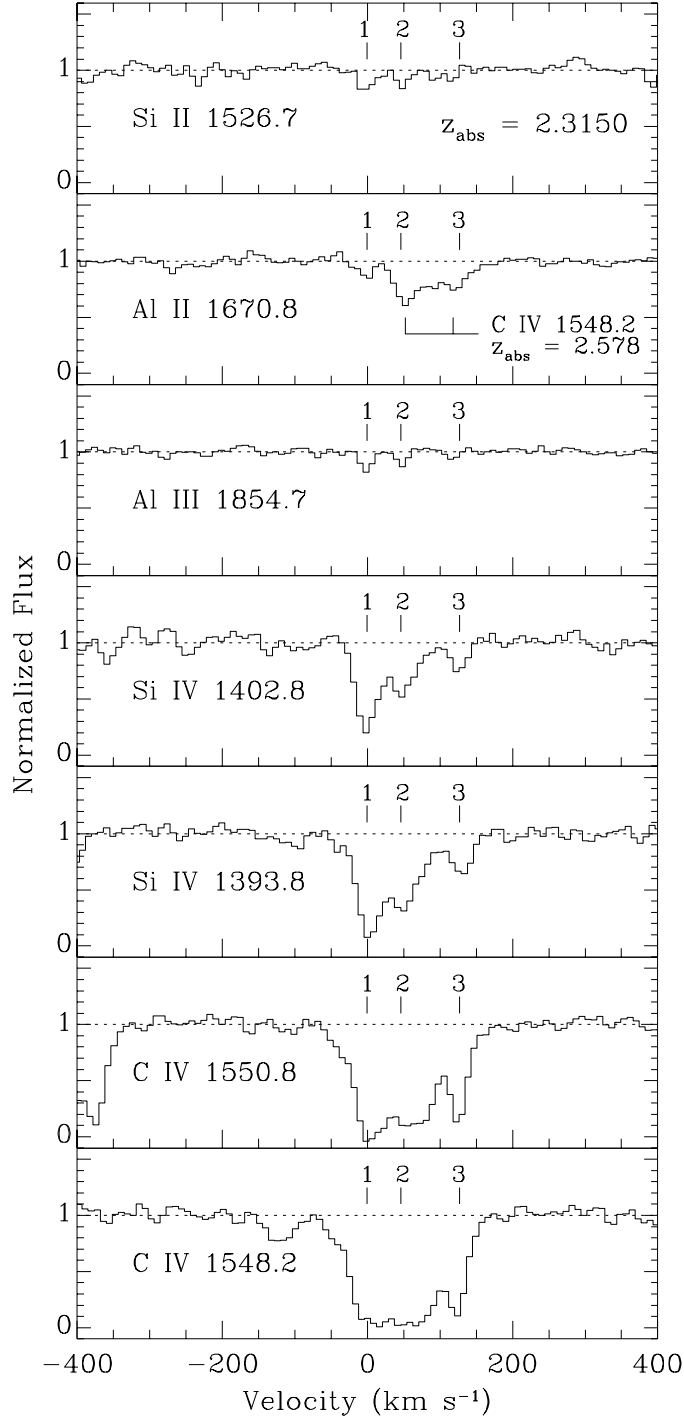


Fig. 2.— Normalized absorption profiles of heavy elements associated with the Lyman limit system at $z_{\text{abs}} = 2.3150$. The profiles are plotted versus restframe velocity with $v = 0 \text{ km s}^{-1}$ at $z = 2.315$. For convenience, we refer to the three resolved components as components 1-3 as marked in each panel. The absorption near components 2 and 3 in the Al II 1670.8 Å profile is predominantly due to C IV at a different redshift (see text §4.8). The absorption feature at $v \approx -120 \text{ km s}^{-1}$ in the C IV 1548.2 Å profile is also probably a line from a different redshift system, although the identification of this line is not secure (§4.7).

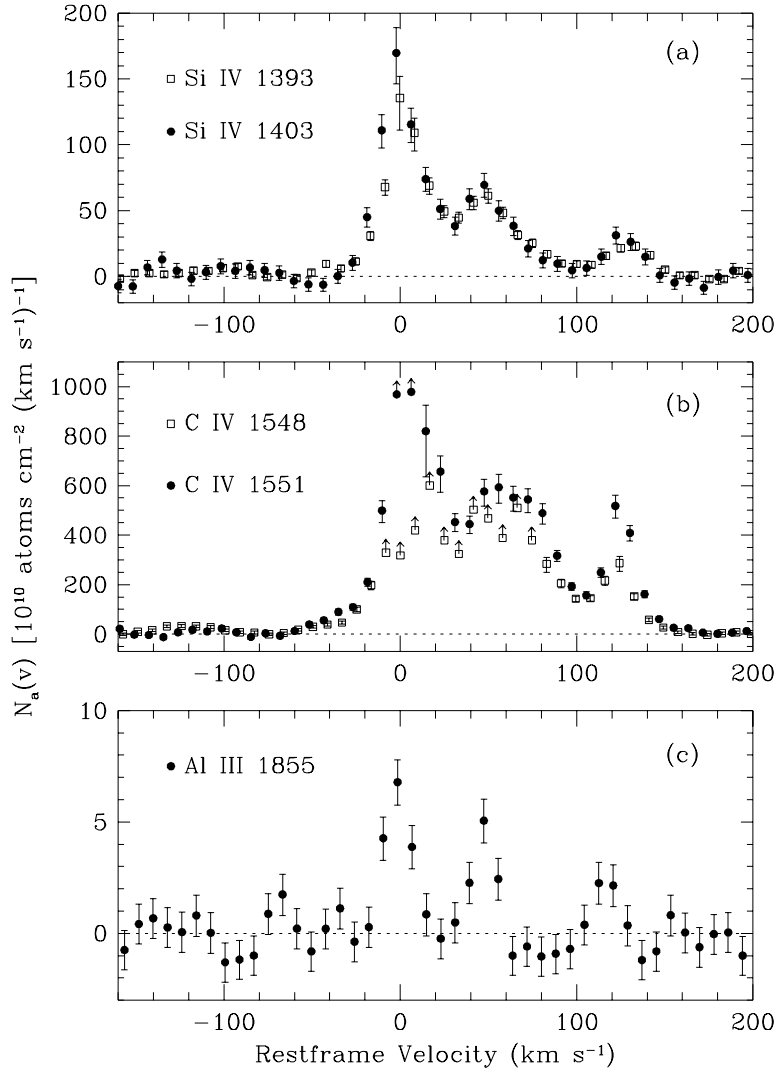


Fig. 3.— Apparent column density profiles (see text §3.2) of heavy elements in the Lyman limit system at $z_{\text{abs}} = 2.3150$: (a) the Si IV 1393.8 and 1402.8 Å lines, (b) the C IV 1548.2 and 1550.8 Å lines, and (c) the Al III 1854.7 Å line. In panels (a) and (b) the stronger member of the doublet is plotted with an open square and the weaker line is indicated with a filled circle.

line. Not surprisingly, this shows that the C IV profile is badly saturated in components 1 and 2. The C IV profile is also significantly saturated in component 3; the weaker line in the C IV doublet (filled circles in Figure 3) yields a significantly higher $N_a(v)$ than the strong line in this component. This high degree of C IV saturation indicates that component 3 is intrinsically rather narrow, and this in turn indicates that the gas is relatively cool. The Si IV profile is less affected by saturation. From Figure 3 we see that the Si IV weak and strong line $N_a(v)$ profiles are in good agreement in components 2 and 3, which indicates that the Si IV column density is reliably measured in these components. In component 1, on the other hand, the weak Si IV line has a higher apparent column density than the strong line, so this component is affected by unresolved saturation. However, Figure 3 indicates that Si IV is only mildly saturated in component 1, so a correction can be applied to the weak line apparent column density to obtain a reliable estimate of $N(\text{Si IV})$ [Savage & Sembach 1991; Jenkins 1996]. Using the method of Savage & Sembach (1991), we estimate that the correction required for the integrated $N_a(v)$ of the Si IV 1402.8 Å line is 0.08 dex. Therefore $\log N_a(\text{Si IV}) = 13.68 + 0.08 = 13.76$ in component 1. This corrected column density is in excellent agreement with the column density from profile fitting, $\log N(\text{Si IV}) = 13.75 \pm 0.07$, which gives us confidence in the measurement. For the Si II, Al II, and Al III profiles we do not have the benefit of additional transitions for $N_a(v)$ comparison, but these lines are all rather weak so saturation is not likely to be a problem. From Figure 3 we see that a very weak absorption feature is present at $v \approx +118 \text{ km s}^{-1}$ in the Al III profile. This is close to component 3 but is shifted slightly blueward compared to Si IV and C IV. Similarly, from Figure 2 we see that there may be weak Si II absorption near but slightly blueward of component 3.

In §5 we discuss the physical conditions in this Lyman limit absorber, and we use standard photoionization models to examine the heavy element abundances.

4.9. $z_{\text{abs}} = 2.37995$

This new metal system is detected only in the C IV 1548.2, 1550.8 Å doublet (lines 26 and 27 in Figure 1 and Table 1). Comparison of the $N_a(v)$ profiles indicates that these C IV lines are not substantially affected by unresolved saturated component structure. Similarly, the C IV column densities from profile fitting and $N_a(v)$ integration agree within the noise, so saturation is not a problem.

4.10. The C IV complex at $2.432 < z_{\text{abs}} < 2.441$

A prominent complex of C IV doublets is detected at $5313 < z_{\text{abs}} < 5336 \text{ Å}$ (lines 28–33 in Figure 1), which corresponds to $2.432 < z_{\text{abs}} < 2.441$. Figure 4 shows an expanded plot of this region of the KPNO spectrum along with the component fit which gives the profile parameters listed in columns 5–7 in Table 1. To show the clustering of C IV lines, we also plot at the top of

Figure 4 the redshifts at which we detect C IV absorbers in the optical spectrum of HS 1700+6416. This absorption complex has two interesting features:

(1) There is a very high density of absorption lines in this small redshift interval. Inspection of the spectrum in Figure 4 reveals that there are at least 4 C IV doublets in this complex within the redshift range $\Delta z = 0.00855$, and this implies that the number of C IV absorbers per unit redshift is $dN/dz \gtrsim 450$. In addition, profile fitting requires a broad component with a substantial column density at $z_{\text{abs}} = 2.43329$; this broad component is not well constrained by the present data and may split up into subcomponents when observed at higher resolution. Also, the strength of the line at 5322.4 Å indicates that another narrow component is present (see below). In contrast, Petitjean et al. (1994) find $dN/dz \approx 7.7$ and Tripp et al. (1996) derive $dN/dz = 7.1 \pm 1.7$ using samples of intervening C IV systems with much larger redshift intervals of $\Delta z = 1.3$ and $\Delta z = 2.4$, respectively. The Petitjean et al. and Tripp et al. samples include *all* C IV lines with rest equivalent width $W_r > 0.03$ Å along multiple sight lines, and therefore these samples provide a measure of the *average* dN/dz of C IV systems at moderately high redshifts. However, Petitjean et al. and Tripp et al. treat any C IV doublets separated by less than 200 km s⁻¹ as a single absorber. Applying this treatment to the data in Figure 4, we still find that there are 2 or 3 C IV systems in this small redshift range implying that $dN/dz > 200$. The high dN/dz measured in this C IV cluster only indicates that the *local* density is very high and is not in conflict with previous estimates of dN/dz over broad redshift intervals.

(2) The weak line (1550.8 Å) of the C IV doublet at $z_{\text{abs}} = 2.43306$ is remarkably well-aligned with the strong line of the C IV doublet at $z_{\text{abs}} = 2.43877$ (see Figure 4). To within what velocity tolerance are these C IV lines aligned? Traditionally the quantity $R = (1 + z_2)/(1 + z_1)$ has been used to search for alignments of absorbers at redshifts z_1 and z_2 ; if the absorbers are aligned in some doublet with wavelengths λ_i and λ_j , then $R = \lambda_i/\lambda_j$. Thus for the C IV doublet we expect $R = 1550.770/1548.195 = 1.001663$, and with $z_1 = 2.433064 \pm 0.000013$ and $z_2 = 2.438767 \pm 0.000013$ we obtain $R = 1.001661 \pm 0.000005$. These redshifts and uncertainties were obtained by fitting the profiles of all lines shown in Figure 4 simultaneously, and the uncertainties in the profile parameters may be greater than the uncertainties formally estimated by the fitting program due to the complexity of the profiles. However, the 1548.2 Å line of the z_1 system and the 1550.8 Å

Fig. 4.— (opposite page) The normalized absorption profiles of the C IV complex at $2.432 < z_{\text{abs}} < 2.441$ (lines 28-33 in Figure 1 and Table 1), plotted versus vacuum Heliocentric wavelength (bottom axis) and velocity in the $z_{\text{abs}} = 2.43877$ rest frame (top axis). The thin histogram shows the observed optical spectrum, and the thick line shows the profile fit which yields the component parameters listed in Table 1. To show the clustering of the C IV absorption systems, and in particular to show the high density of C IV doublets in this redshift range, we plot the redshifts of all detected C IV doublets (not including lines in the Ly α forest) at the top of the figure. Here each C IV doublet is indicated with a single thin vertical line at the measured redshift. The line identification numbers from Table 1 are shown at the bottom of the lower panel.

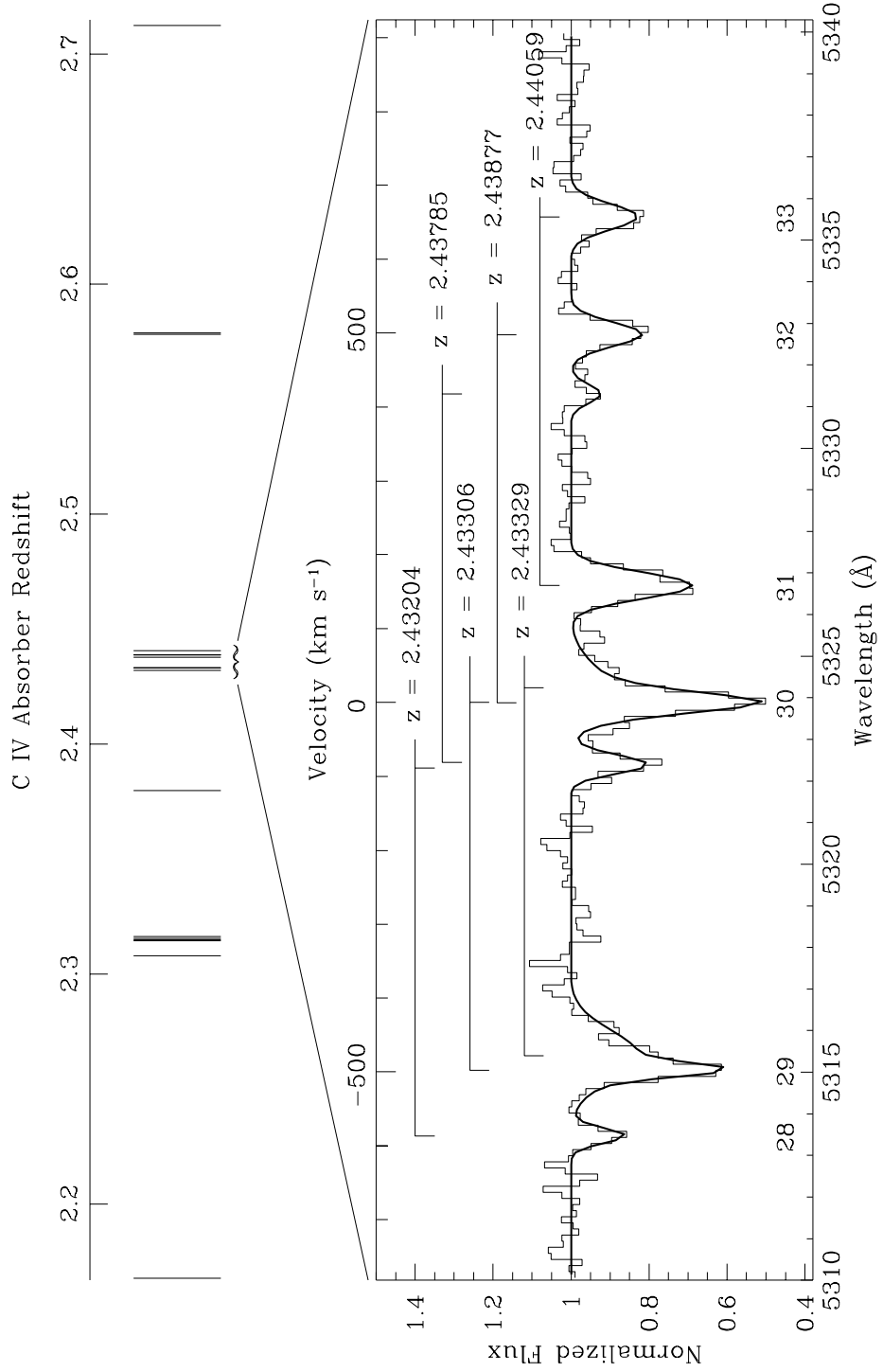


Fig. 4.— continued

line of the z_2 system are free from confusion from this alignment, so independently fitting these lines provides an estimate of the redshifts which is not affected by the severe blending due to the redshift overlap. The z_1 1548.2 Å line is blended with a broad component at $z \approx 2.4333$ (see Figure 4), and it is necessary to fit the broad component and z_1 simultaneously to obtain an acceptable fit, but the core of the z_1 line is narrow and deep enough that z_1 is well-constrained despite the blend. The z_2 1550.8 Å line is not blended. From this independent fitting exercise, we obtain $z_1 = 2.433055 \pm 0.000016$ and $z_2 = 2.438787 \pm 0.000019$. From these redshifts we estimate that z_1 and z_2 are aligned to within 10 km s^{-1} at the 3σ level.

There is another pair of weak C IV doublets in Figure 4 which show the weak line of one absorber aligned with the strong line of another, although this case is not as strong. The line at 5313.49 Å is attributed to C IV 1548.2 at $z_{\text{abs}} = 2.43204$. The corresponding weak (1550.8 Å) line is detected at the expected wavelength (5322.3 Å), but it is considerably stronger than the 1548.2 Å line, and fitting the profiles of the 5313.5 and 5322.3 Å lines with only one component yields a very poor fit. Since the line at 5313.5 only allows one component, we attribute the line at 5322.3 Å to the 1550.8 Å line at $z_{\text{abs}} = 2.43204$ blended with a C IV 1548.2 Å line at $z_{\text{abs}} = 2.43785$, and we find that there is a weak absorption line at the expected wavelength of C IV 1550.8 Å at $z_{\text{abs}} = 2.43785$. Since these doublets are weaker than the aligned doublets discussed in the previous paragraph, we cannot constrain the velocity alignment as tightly. We estimate that the weak line of the $z_{\text{abs}} = 2.43204$ absorber is aligned to within $\sim 25 \text{ km s}^{-1}$ with the strong line of the $z_{\text{abs}} = 2.43785$ absorber.

This alignment of the weak C IV line from one redshift with the strong C IV line from a different redshift is reminiscent of the absorption “line locking” phenomenon which was once a topic of considerable interest and controversy (Perry, Burbidge, & Burbidge 1978; Weymann, Carswell, & Smith 1981 and references therein). Some interesting examples of aligned weak and strong doublet lines from different redshift systems have appeared in more recent literature (e.g., Foltz et al. 1987; Wampler 1991; Wampler, Bergeron, & Petitjean 1993). In some cases these occur in broad absorption line (BAL) and “associated” absorption systems with $z_{\text{abs}} \approx z_{\text{em}}$, which is perhaps not surprising since radiative acceleration provides a natural explanation of these alignments, and the presumably close proximity of the $z_{\text{abs}} \approx z_{\text{em}}$ absorbers to the QSO would subject them to an extreme non-isotropic radiation field. Several models of BAL outflows have recently been proposed in which radiation pressure plays a critical role (e.g., Arav, Li, & Begelman 1994; Murray et al. 1995; Scoville & Norman 1995), and Arav et al. (1995) have shown that a double-trough spectral signature predicted by their model is convincingly detected in the types of QSOs where it is expected to be present. However, the C IV complex shown in Figure 4 is definitely not a BAL system, and it is displaced from z_{em} by $\sim 24000 \text{ km s}^{-1}$, so it usually would not be considered an associated system either. BAL outflows do attain velocities this large (Turnshek 1988), so perhaps this C IV complex is close to the QSO and was accelerated in an earlier BAL outflow that has since mostly dissipated (a scenario proposed by Turnshek 1988). Alternatively, this may be a BAL outflow which is just beginning to form with the high velocity

absorption showing up first to be followed later by lower velocity absorption with z_{abs} closer to z_{em} .

Before pursuing these speculations, it is important to ascertain whether or not the doublet alignments in Figure 4 could simply be coincidental. If we consider randomly placing some number of C IV absorbers in a specified velocity interval, then we can use the binomial distribution to estimate the probability that the weak line of one absorber could by chance be aligned with the strong line of a different absorber to within some velocity tolerance. It is not immediately obvious what velocity interval or number of absorbers should be assumed for this calculation, however, and these assumptions significantly affect the probability. The *minimum* velocity interval (which translates to an *upper limit* on the probability) is the difference between the velocity of the strong line of the highest redshift doublet in the cluster and the velocity of the strong line of the lowest redshift doublet (if the velocity interval were less than this, then the C IV complex shown in Figure 4 would never occur because some of the doublets would be outside of the velocity interval). This corresponds to a wavelength interval of $\Delta\lambda = 13.2 \text{ \AA}$ or a velocity interval of $\Delta v = 746 \text{ km s}^{-1}$. There are four well-detected absorbers ($z_{\text{abs}} = 2.43204, 2.43306, 2.43877,$ and 2.44059) in this λ range, and as noted above, it is likely that there is another at $z_{\text{abs}} = 2.43785$, and there is a broad component at $z_{\text{abs}} = 2.43329$ which could be due to multiple blended C IV lines. With four absorbers and $\Delta v = 746 \text{ km s}^{-1}$, the probability of one weak/strong line alignment to within 10 km s^{-1} is 15%. If we include the second apparent weak/strong line alignment, then we must relax the velocity overlap tolerance to 25 km s^{-1} , and we must randomly place at least five absorbers in the velocity interval, so in this case the probability of two chance alignments is 12%. If we increase the number of absorbers to, say, 7, then the probability of two alignments to within 25 km s^{-1} increases to 28%.

Evidently it is possible that these apparently line locked systems are just chance coincidences in an overdense C IV complex. Nevertheless, since similar highly displaced line alignments have been reported elsewhere (Wampler et al. 1993), it is worthwhile to make a note of this. If highly displaced line alignments show up in future high resolution QSO absorber studies, then this may reveal an interesting new QSO phenomenon or evolutionary stage. It is also interesting to note that Sargent, Boksenberg, & Steidel (1988), Hamann, Barlow, & Junkkarinen (1997a), and Jannuzi et al. (1996) have reported evidence of a new class of QSO absorption systems which are similar to BALs but highly displaced from the QSO systemic redshift and lacking the $z_{\text{abs}} \approx z_{\text{em}}$ absorption usually detected in BALs. These displaced BALs may be related to the C IV complex discussed in this section. It may be possible to establish that this C IV complex is close to the QSO by monitoring the absorption profile; if the profile shows temporal variability, then the absorbing gas must be close to the QSO.

4.11. $z_{\text{abs}} = 2.57813, 2.57884$

Reimers et al. (1992) report detection of this system in several metals, but they do not detect Lyman limit absorption. However, the spectral coverage of the FOS observation barely reaches the expected wavelength of this Lyman limit, and their S/N drops off precipitously in this region (see Figure 1 in Vogel & Reimers 1995), so the FOS spectrum is not sensitive to Lyman continuum absorption at this redshift. We detect the C IV 1548.2, 1550.8 Å doublet in this system, and two components are obvious in the profiles of both lines (see lines 36 and 37 in Figure 1). Comparison of the $N_{\text{a}}(v)$ profiles of the C IV doublet does not show unresolved saturation in either component. The C IV 1548.2 Å profile shows a third component, but there is no evidence of this component in the 1550.8 Å profile and, as discussed above, this third component⁹ may be Al II 1670.8 at $z_{\text{abs}} = 2.3150$. The $z_{\text{abs}} = 2.3150$ system shows complex component structure (see Figure 2), so the C IV 1548.2 profile could be contaminated with Al II absorption from $z_{\text{abs}} = 2.3155$.

4.12. $z_{\text{abs}} = 2.7125$

Reimers et al. (1992) and Vogel & Reimers (1995) do not report detections of any metals at this redshift, but as discussed by Petitjean et al. (1996), some of the heavy element lines at this redshift in the FOS spectrum may have been misidentified by Vogel & Reimers. For example, Petitjean et al. point out that the line Vogel & Reimers attribute to O II 833.3 Å at $z_{\text{abs}} = 2.433$ could instead be Ne VIII 770.4 Å at $z_{\text{abs}} = 2.712$. In the KPNO optical spectrum we detect the N V 1238.8, 1242.8 Å and C IV 1548.2, 1550.8 Å doublets at this redshift (see lines 3-4 and 38-39, respectively, in Table 1 and Figure 1). A 4.7σ absorption line is present at 4842.45 Å, the expected wavelength of Si II 1304.4 Å at $z_{\text{abs}} = 2.71249$. However, this identification probably is not correct because other Si II lines should be detected as well, and they are not. For example, the Si II 1260.4 Å line is considerably stronger than the 1304.4 Å line, but the 1260.4 Å line is not detected. There is a weak unidentified feature recorded at 4679.89 Å (line 8 in Figure 1), but this is shifted redward from the expected wavelength of the Si II 1260.4 Å line by $\Delta z = +0.00047$, and furthermore this unidentified line is much weaker than the expected Si II 1260.4 Å line (based on the strength of the line at 4842.45, assuming it is due to Si II 1304.4 Å). Similarly, the Si II 1526.7 Å line should be easily detected, but no line is apparent at the expected wavelength (see Figure 1).

The apparent column density profiles of the C IV and N V doublets at $z_{\text{abs}} = 2.7125$ are shown in Figure 5. This figure suggests that the N V absorption profile is affected by unresolved saturation; the weak N V line (1242.8 Å) has a significantly higher $N_{\text{a}}(v)$ than the strong line in the core of the profile, and the integrated N V 1242.8 Å column density, $\log N(\text{N V}) = 13.87$, is 0.09 dex greater than the integrated column of the 1238.8 Å line. Alternatively, Figure 5

⁹If the third component is due to C IV at $z_{\text{abs}} = 2.57746$ rather than Al II, then from profile fitting we obtain $b = 7.3 \text{ km s}^{-1}$ and $\log N(\text{C IV}) = 12.66$.

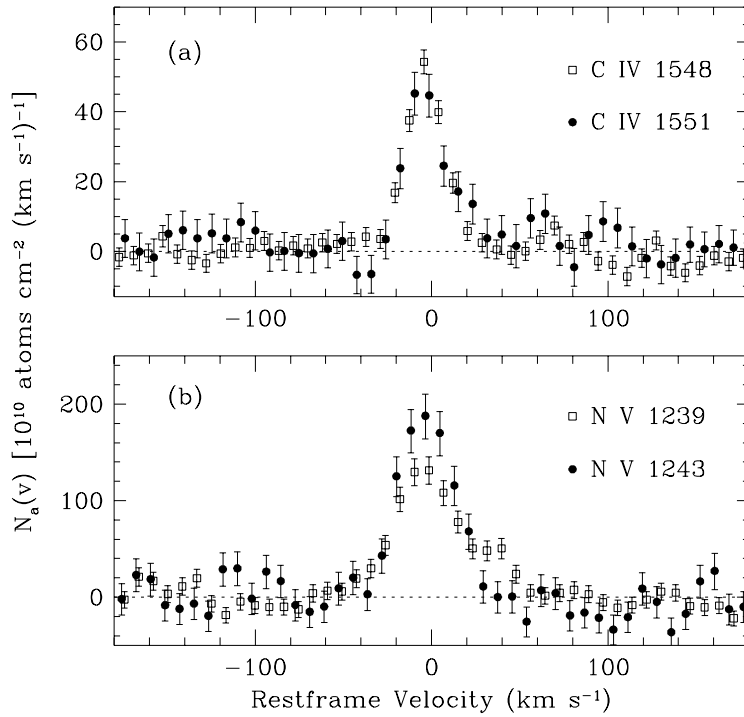


Fig. 5.— Apparent column density profiles (§3.2) of (a) the C IV 1548.2 and 1550.8 Å lines and (b) the N V 1238.8 and 1242.8 Å lines of the associated absorber at $z_{\text{abs}} = 2.7125$. The stronger line of each doublet is plotted with an open square and the weaker line with a filled circle. The $N_a(v)$ profiles of the weak and strong C IV lines are in good agreement, which indicates that C IV is not affected by unresolved saturation in this absorber. However, in the core of the profile, the weaker N V line yields a significantly higher $N_a(v)$ than the strong line. This indicates that either the N V profile is affected by unresolved saturated absorption, or the absorbing gas does not completely cover the QSO flux source.

may indicate that the N V absorbing gas does not completely cover the flux source (see below). The column density from profile fitting agrees with the integrated 1242.8 Å column density, but inspection of the fitted profiles shows that the fit is not very good and the observed optical depth in the core of the 1242.8 Å line exceeds the profile fit, so the true column density could be somewhat higher. From Figure 5 we see that C IV, on the other hand, is not significantly affected by unresolved saturation (or incomplete covering) at this redshift; the C IV weak and strong line $N_a(v)$ profiles are in good agreement as are the column densities from profile fitting and $N_a(v)$ integration (see Table 1).

This absorption system occurs within 5000 km s⁻¹ of the QSO emission redshift and thus qualifies as an “associated” absorber. There are some indications that these are a special class of QSO absorbers which may be intrinsically related to the QSO nucleus or host galaxy, but there is also evidence that some absorption systems within 5000 km s⁻¹ of z_{em} are at least a few hundred kpc away from the QSO (Turnshek, Weymann, & Williams 1979; Morris et al. 1986; Tripp et al. 1996). Probably this class of absorbers includes a mix of intrinsic and intervening absorption systems. In §5.2.3 we use photoionization models to study the abundances and ionization in this absorption system. Recently it has been suggested that the gas in some associated absorbers does not completely cover the QSO flux source (Wampler et al. 1993; Petitjean et al. 1994; Hamann et al. 1997a,b; Barlow & Sargent 1997). If this is true, then these associated absorbers must be close to the QSO nucleus. The case presented by Barlow & Sargent (1997) is particularly convincing because the H I Ly α profile has an obvious flat bottom indicative of strong saturation, but the flux in the flat bottom of the profile is well-detected and is not zero. While quite interesting, this complicates the column density measurements because even if the lines are unsaturated, the incomplete covering will introduce errors in column densities from profile fitting and $N_a(v)$ integration. The discrepancy between the N V 1238.8 and 1242.8 Å $N_a(v)$ profiles shown in Figure 5 could indicate that the absorbing gas does not completely cover the flux source. In principle, one can attempt to correct the absorption profiles for partial covering (c.f., Hamann et al. 1997b; Barlow & Sargent 1997), but in this case this is difficult since the absorption lines are strong enough that a mix of partial covering and saturation could affect the measurements. For the N V column densities in the $z_{\text{abs}} = 2.7125$ absorber, we adopt the conservative approach of simply treating the integrated column density of the weak line as a lower limit on $N(\text{N V})$.

5. Physical Conditions and Abundances

In this section we examine the physical conditions and abundances in the metal systems of HS 1700+6416. We begin with simple inferences drawn from the absorption line measurements, and then we apply standard photoionization models to estimate abundances. However, we find some indications that the standard single-zone photoionization models are too simple to explain the data and multi-zone models may be required (see below).

5.1. Temperature and Ionization

The observed line widths provide one of the most straightforward probes of physical conditions. If the absorption profile is dominated by Doppler broadening (i.e., thermal motions), then the temperature T of the gas can be calculated from the measured Doppler parameter, $b = \sqrt{2}\sigma = 0.129\sqrt{T/A}$, where A is the atomic weight of the element and σ is the radial velocity dispersion of the gas (Spitzer 1978). In QSO absorbers, the gas is often cool enough that other factors such as bulk motions, turbulence, or multiple unresolved components can significantly broaden the line, so the temperature derived from this equation must be treated as an upper limit¹⁰. Since b goes as $A^{-1/2}$, lighter elements like carbon are more useful for constraining the temperature of the gas. In Table 3 we list upper limits on the gas temperature derived from the Doppler parameters¹¹ of all C IV lines detected in the KPNO optical spectrum.

An issue of considerable interest is the question of the ionization mechanism(s) in the various types of QSO absorbers. Are intervening QSO absorbers photoionized by the UV background radiation from QSOs and AGNs, or do local photoionizing sources and/or collisional ionization play a role? From Table 3 we see that four of the C IV absorption lines in the HS 1700+6416 optical spectrum have $T < 50000$ K. At these temperatures very little C IV is present in gas in collisional ionization equilibrium (Sutherland & Dopita 1993), so these systems are probably photoionized. However, it is also possible that the narrow C IV lines occur in nonequilibrium gas which has cooled more rapidly than it has recombined; this is predicted in some renditions of galactic fountain theory (Edgar & Chevalier 1986; Benjamin & Shapiro 1997). It is important to note that in some cases these lines are moderately weak and noise could cause the profiles to appear artificially narrow. On the other hand, some of the C IV lines are so broad as to indicate that the line profiles are probably *not* dominated by thermal Doppler broadening. For example, the C IV absorber at $z_{\text{abs}} = 2.57884$ has $b = 35.0 \pm 3.8$ km s⁻¹, which implies that $T \approx 10^{5.9}$ K if the profile is dominated by thermal motions; at this temperature carbon is predominantly in higher ionization stages than C IV in collisional ionization equilibrium (Sutherland & Dopita 1993).

The high ion column density ratios in the Lyman limit absorber at $z_{\text{abs}} = 2.3150, 2.3155$ indicate that the ionization conditions differ significantly from the conditions in the gaseous halo of the Milky Way. From Figure 3 we see that $N(\text{C IV})/N(\text{Si IV}) \geq 10$ in components 2 and 3 of this absorber and could be significantly larger since the C IV profile is affected by strong saturation. For comparison, Sembach & Savage (1992) measure $N(\text{C IV})/N(\text{Si IV}) = 3.6 \pm 1.3$ in the Milky Way gaseous halo. More recently Sembach, Savage, & Tripp (1997) have compiled the

¹⁰However, in a recent Keck study of a large number of C IV QSO absorbers, Rauch et al. 1996 conclude that most C IV profiles are dominated by thermal motions.

¹¹Doppler parameter uncertainties could be larger than the formal fitting errors suggest since the true absorption profiles may be kinematically more complex than the simple one component Voigt profile assumed. This is particularly true for strongly blended adjacent components and narrow components with b substantially smaller than the 20 km s⁻¹ resolution.

Table 3. Temperature Upper Limits from C IV Lines^a

z_{abs}	b (km s ⁻¹)	T (K)
2.16797	16.5±0.8	<2.0×10 ⁵
2.30812	25.0±2.2	<4.7×10 ⁵
2.31458 ^{b,c}	14.6±5.4	<1.5×10 ⁵
2.31505 ^{b,c}	11.3±3.8	<9.2×10 ⁴
2.31568 ^{b,c}	28.6±1.5	<5.9×10 ⁵
2.31638 ^{b,c}	3.9±0.2	<1.1×10 ⁴
2.37995	6.3±2.0	<2.9×10 ⁴
2.43204 ^b	8.0±5.5	<4.6×10 ⁴
2.43306 ^b	4.0±3.5	<1.2×10 ⁴
2.43329 ^b	44.5±4.9	<1.4×10 ⁶
2.43785 ^b	12.6±4.3	<1.1×10 ⁵
2.43877 ^b	18.3±1.9	<2.4×10 ⁵
2.44059	20.3±1.7	<3.0×10 ⁵
2.57813 ^b	18.9±1.9	<2.6×10 ⁵
2.57884 ^b	35.0±3.8	<8.8×10 ⁵
2.71245	11.4±1.1	<9.4×10 ⁴

^aTemperature upper limits derived from the Doppler parameter, $b = 0.129\sqrt{T/A}$. The atomic weight of carbon is $A = 12.0111$. The temperature estimates assume the absorption lines are well represented by single component Voigt profiles unless otherwise noted.

^bBlended absorption line.

^cSaturated absorption line.

best measurements made with the *HST* and *International Ultraviolet Explorer (IUE)* of high ion column densities in the Galactic ISM, and they find $N(\text{C IV})/N(\text{Si IV}) = 3.8 \pm 1.9$ with the vast majority of the ISM C IV/Si IV ionic ratios being well below 10 (see their Figure 8). This high ionic ratio in the LL absorber is not expected on the basis of cooling galactic fountain theory but could be produced in supernova remnants, conductive interfaces between warm and hot gas, or “turbulent mixing layers” (see §8 in Sembach et al. 1997 and references therein). This higher ratio could also be due to the significantly increased intensity of the extragalactic UV background radiation at $z \approx 2$ compared to $z \approx 0$ (c.f., Bechtold 1995 and references therein).

Since the temperature of the gas producing the C IV absorption line in this LL absorber at $z_{\text{abs}} = 2.31638$ (i.e., component 3, see Figure 2) is evidently less than roughly 11000 K (Table 3), it seems likely that this system is photoionized. Components 1 and 2 may or may not be photoionized (the line widths are large enough to allow collisional ionization), but given the small total H I column density for all components derived from τ_{LL} by Reimers et al. (1992) [$\log N(\text{H I}) = 16.85$], photoionization by the extragalactic UV background radiation is likely to be significant in all three components (c.f., Viegas 1995), so modeling is required to estimate elemental abundances.

5.2. Photoionization Models

Following the seminal paper of Bergeron & Stasińska (1986), it has become customary to use photoionization models to infer abundances in moderate column density QSO absorbers, and the physical conditions discussed above indicate that this is appropriate. In this section we use models constructed with the photoionization code CLOUDY (version 84.12; Ferland 1993) to estimate the abundances in the Lyman limit and associated absorption systems. We model the LL absorbers as a constant density plane parallel slab photoionized predominantly by the Madau (1992) extragalactic background radiation from QSOs/AGNs, which includes the effects of H and He opacity in intervening Ly α clouds and Lyman limit systems. The slab is illuminated on one side. We assume the mean intensity at the hydrogen Lyman limit is $J_{\nu}(\text{LL}) = 10^{-21}$ ergs $\text{s}^{-1} \text{cm}^{-2} \text{Hz}^{-1} \text{sr}^{-1}$. For the associated absorber, the model assumes the gas is predominantly photoionized by the flux from HS 1700+6416 itself (see §5.2.3). Once the radiation field has been specified, other parameters which can be modified to fit the observed column densities are the overall metallicity [M/H], the relative heavy element abundances, the ionization parameter Γ ($\equiv n_{\gamma}/n_{\text{H}} = \text{H ionizing photon density}/\text{total hydrogen number density}$), and the H I column density. We express the logarithmic abundance of element X relative to element Y using the usual notation, $[X/Y] = \log(X/Y) - \log(X/Y)_{\odot}$, and we use [M/H] to indicate the overall abundance of the metals relative to solar. Throughout this paper we use the solar abundances from Grevesse & Anders (1989).

We begin by placing lower limits on the heavy element abundances, and then for absorbers detected in several species and ionization stages, we use the models to more tightly constrain the

metallicities. As discussed by Hamann (1997), even if we have measured column densities of *only one* ionization stage of metal X (e.g., Mg II) and H I, we can still place a lower limit on [X/H] in the context of the photoionization model. The abundance [X/H] can be expressed as

$$\left[\frac{\text{X}}{\text{H}}\right] = \log\left(\frac{N(\text{X}_i)}{N(\text{H I})}\right) + \log\left(\frac{f(\text{H I})}{f(\text{X}_i)}\right) - \log\left(\frac{\text{X}}{\text{H}}\right)_\odot \quad (3)$$

where X_i is element X in ionization stage i , N is the column density, f is the ionization fraction, and $(\text{X}/\text{H})_\odot$ is the abundance ratio in the sun. By choosing the model ionization parameter which minimizes $f(\text{H I})/f(\text{X}_i)$, we can derive a lower limit on [X/H]; any other value of Γ will lead to higher [X/H]. In practice our method is to calculate $N(\text{X}_i)$ vs. Γ for a series of models with decreasing values of [X/H] and fixed $N(\text{H I})$; eventually [X/H] drops low enough so that the peak of the $N(\text{X}_i)$ vs. Γ curve is lower than the observed column density of X_i . For several of the HS 1700+6416 LL absorbers, Table 4 summarizes the lower limits on [X/H] which agree with the measured column densities, to within the 2σ uncertainties, at the peak of the $N(\text{X}_i)$ vs. Γ curve calculated by the model described above.

5.2.1. Lyman Limit Absorber at $z_{\text{abs}} = 2.3150, 2.3155$

The abundance lower limits derived using equation 3 as discussed above are $[\text{Si}/\text{H}] \geq -0.95$ and $[\text{Al}/\text{H}] \geq -0.96$ in component 1 ($z_{\text{abs}} = 2.3150$) and $[\text{Si}/\text{H}] \geq -1.35$ and $[\text{Al}/\text{H}] \geq -1.40$ in component 2 ($z_{\text{abs}} = 2.3155$). These lower limits were calculated assuming $\log N(\text{H I}) = 16.85$ for each component. There are at least three absorption components in this LL system (see Figure 2), and $\log N(\text{H I}) = 16.85$ is the *total* H I column (i.e., integrated across all components) derived from the Lyman limit optical depth. Therefore these are rather conservative lower limits; $N(\text{H I})$ in the *individual* components is almost certainly lower than the assumed value so the abundances are almost certainly higher than these lower limits.

In this absorber we detect absorption lines from several species including multiple ionization stages of Si and Al (see Table 2), so we may be able to more accurately pin down the abundances using photoionization models which simultaneously match all of the measured heavy element column densities. However, with these models one must bear in mind that different ionization stages such as Si II and Si IV may not occur in the same gas, i.e., the absorber may be a multiphase medium. We will start with the single zone model in which all of the absorption lines are assumed to arise in the same gas because it is the simplest model. With this caveat, consider component 1 ($z_{\text{abs}} = 2.3150$). Based on the heavy element column densities, we estimate that $\log N(\text{H I}) \approx 16.6$ for component 1 assuming components 1 and 2 have roughly the same metallicity and contain the bulk of the neutral hydrogen. Our best estimations of the metal column densities in this component are $\log N(\text{Si II}) = 13.07 \pm 0.12$, $\log N(\text{Al II}) = 11.69 \pm 0.11$, $\log N(\text{Al III}) = 12.11 \pm 0.09$, and $\log N(\text{Si IV}) = 13.75 \pm 0.07$ (see §4.8). A very crude lower limit of $\log N(\text{C IV}) > 14.6$ is obtained by integrating the apparent column density of C IV 1550.8 Å over the velocity range of component 1.

Table 4. Lower Limits on Heavy Element Abundances^a

<u>Lyman Limit Absorbers</u>					
z_{abs}	$\left[\frac{\text{Mg}}{\text{H}}\right]$	$\left[\frac{\text{C}}{\text{H}}\right]$	$\left[\frac{\text{N}}{\text{H}}\right]$	$\left[\frac{\text{Si}}{\text{H}}\right]$	$\left[\frac{\text{Al}}{\text{H}}\right]$
1.15729	≥ -0.22
1.84506	≥ -0.45	≥ -2.26
2.16797	...	≥ -2.81
2.31499	$\geq -0.95^{\text{b}}$	$\geq -0.96^{\text{c}}$
2.31551	$\geq -1.35^{\text{b}}$	$\geq -1.40^{\text{c}}$
<u>Associated Absorber – Model 1^d</u>					
2.7125	...	≥ -0.82	≥ -0.65
<u>Associated Absorber – Model 2^d</u>					
2.7125	...	≥ -0.25	$\geq +0.19$

^aThese abundance lower limits were derived using equation 3 as discussed in the text, §5.2.

^bLower limit derived from $N(\text{Si II})$.

^cLower limit derived from $N(\text{Al III})$.

^dTwo models were used to place lower limits on the associated absorber abundances. Model 1 used the observed QSO spectral energy distribution to set the model continuum shape while Model 2 used continuum shape ‘A’ from Hamann (1997) with $\log T_c = 5.7$.

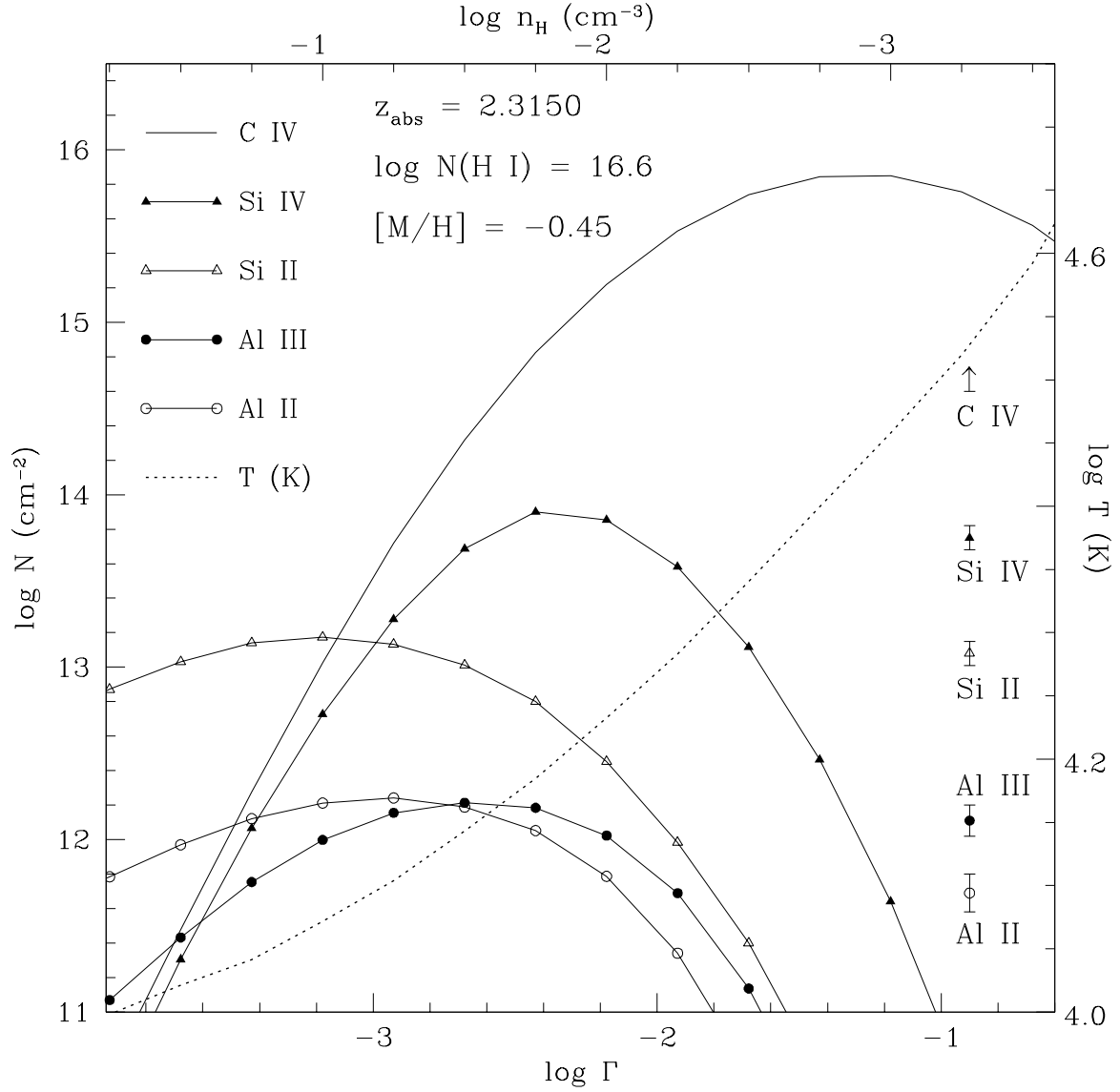


Fig. 6.— Column densities predicted by a photoionized model of the Lyman limit absorber at $z_{\text{abs}} = 2.3150$ (see text §5.2.1) as a function of ionization parameter Γ (bottom axis) and total hydrogen number density n_{H} (top axis). The column densities of heavy elements detected in component 1 of the Lyman limit system ($z_{\text{abs}} = 2.3150$) are shown at right with 1σ error bars; C IV is strongly affected by absorption saturation. The dotted line shows the model temperature vs. Γ with the temperature scale on the right axis.

To simultaneously produce enough Si II and Al II in component 1 with $\log N(\text{H I}) = 16.6$ (ignoring for the moment the higher ionization stages), the model must have $[\text{M}/\text{H}] \geq -0.73$. Since Si II and Al II are the dominant ionization stages of Si and Al in interstellar H I regions, this lower limit holds even if the higher ion absorption does not occur in the same gas. However to simultaneously match $N(\text{Si II})$ and $N(\text{Si IV})$, the model must have a higher metallicity. To search for a model which agrees with *all* of the observed column densities, we have carried out a series of CLOUDY calculations with metallicities ranging from $[\text{M}/\text{H}] = -0.60$ to $[\text{M}/\text{H}] = -0.30$. Figure 6 shows a sample CLOUDY calculation, and Figure 7 summarizes the results of these modeling efforts. Figure 6 shows the column densities of these species, as a function of Γ , calculated by a photoionization model with $[\text{M}/\text{H}] = -0.45$. We present this particular CLOUDY calculation as a sample because this model provides the single best fit. From the figure we see that the model is consistent with the observed column densities of Si II, Al III, and Si IV, to within the 2σ uncertainties, when $-2.73 \leq \log \Gamma \leq -2.46$, and it is consistent with the lower limit on $N(\text{C IV})$ when the ionization parameter exceeds -2.54 . The dashed line in Figure 6 shows the mean temperature of the model as a function of Γ , and we see that in this ionization parameter range the model is also in agreement with the observational constraints on the gas temperature. However, over this ionization parameter range the calculation predicts too much Al II by 0.4–0.5 dex, which is greater than the 3σ uncertainty of $N(\text{Al II})$. This problem is aggravated by the possible contamination of the Al II absorption from C IV 1548.2 Å at $z_{\text{abs}} = 2.57746$ (see §4.8 and Figure 2); if this absorption is partly or mostly due to C IV at a different redshift, then the discrepancy between the model and the observed $N(\text{Al II})$ is even greater.

Figure 7 summarizes the results from five photoionization models with $-0.60 \leq \log \Gamma \leq -0.40$. For each species, the labeled horizontal bar in Figure 7 shows the ionization parameter range which yields model column densities in 2σ agreement with the measured values. From Figure 7 we see that *none* of the models are able to fit all of the observed column densities for any value of Γ . Models with $-0.50 \lesssim [\text{M}/\text{H}] \lesssim -0.40$ can fit all of the species except Al II. When $[\text{M}/\text{H}]$ exceeds -0.40 , the model fails to fit several of the observed column densities at any given value of Γ . There are several possible explanations for the difficulty in fitting Al II including the following. (1) Aluminum could be underabundant in the gas-phase relative to Si and C, due either to depletion onto dust grains or relative metal abundances which are intrinsically different from solar. In the ISM of the Milky Way, aluminum is strongly depleted from the gas-phase by incorporation into dust grains (Jenkins 1987) while Si and C are moderately or lightly depleted (Sofia, Cardelli, & Savage 1994), and therefore depletion could cause Al to be underabundant. Alternatively, the intrinsic Al/Si and Al/C abundances could be different from solar. In low metallicity stars in the Milky Way halo, Si is overabundant relative to aluminum, and this is attributed to different nucleosynthesis time scales for Si and Al (McWilliam et al. 1995; Ryan, Norris, & Beers 1996; Wheeler, Sneden, & Truran 1989 and references therein). Either of these phenomena could alleviate the problem with Al II in the model. If Al is underabundant by ~ 0.2 dex relative to Si and C, for example, then the model shown in Figure 6 could fit all of the metal column densities at $\log \Gamma = -2.54$. (2) The absorption lines could arise in a multiphase medium in which the low

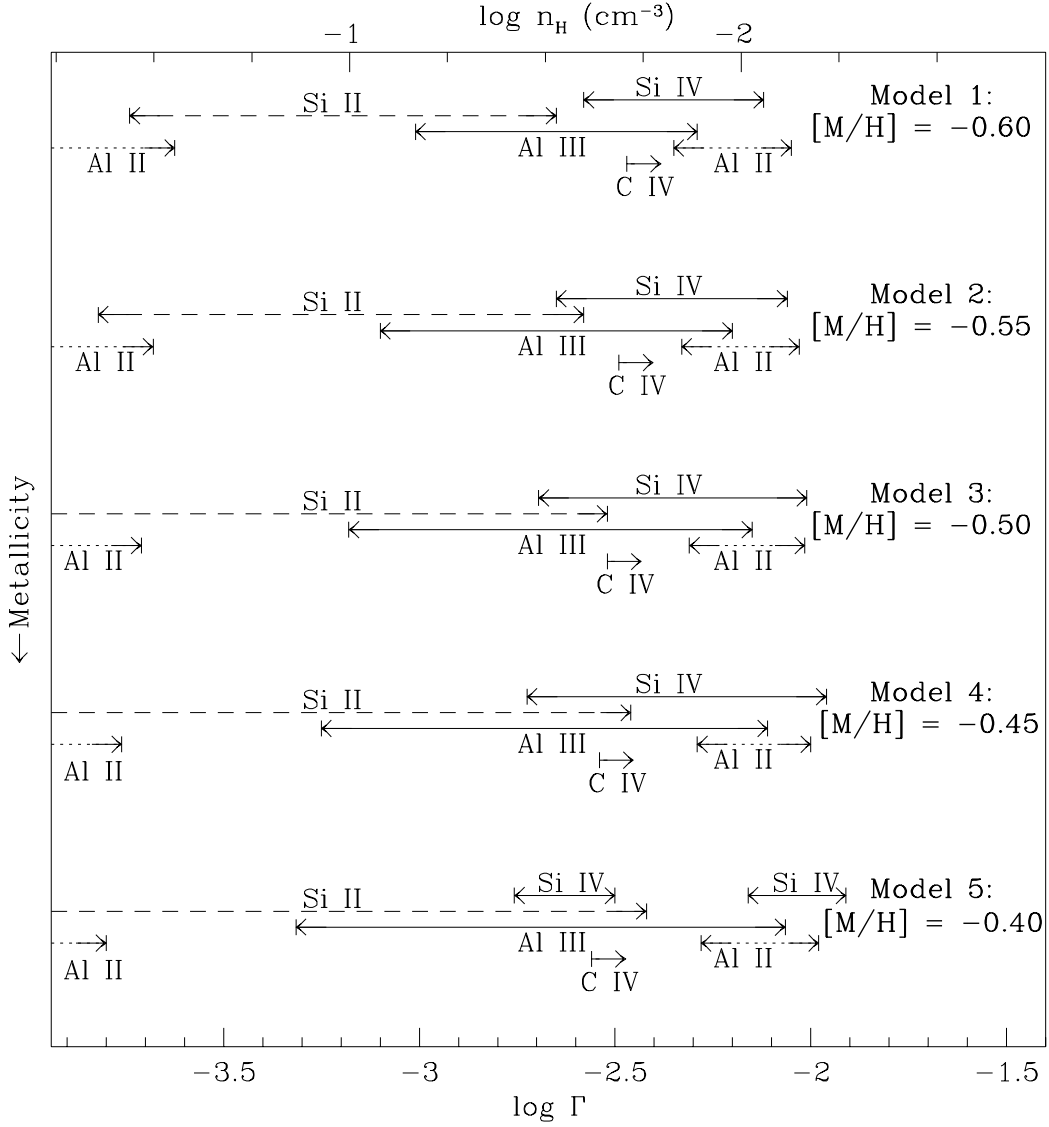


Fig. 7.— Summary of photoionization modeling results for the Lyman limit absorber at $z_{\text{abs}} = 2.3150, 2.3155$. Five models are shown with metallicities ranging from $[M/H] = -0.60$ to $[M/H] = -0.40$. For each observed species, a horizontal bar indicates the range of ionization parameter Γ over which the model is in agreement with the measured column density to within the 2σ uncertainties. For convenience in distinguishing the various species, the ionization parameter range is indicated with a dashed line for Si II and a dotted line for Al II. Note that for some species (e.g., Al II) there are multiple ranges of Γ which are in agreement with the measured column densities. None of these models which assume solar relative abundances are able to simultaneously fit all of the observed column densities for any value of the ionization parameter.

ionization species are associated with the H I but some or all of the higher ion absorption occurs in a physically distinct region. In this case the single-zone models of Figures 6 and 7 are not expected to succeed; more complex multi-zone models are required. (3) There may be some problems with the Al atomic data in the model, especially the Al dielectronic recombination rates (see §4.1 in Petitjean et al. 1994). (4) We may be deceived by noise since the Al II line is marginally detected.

The presence of multiple components in this absorber suggests that it may not be appropriate to model the total column densities as a single constant density slab; the multiple components indicate that the density changes along the line of sight. However, some previous studies of abundances in Lyman limit absorbers (e.g., Vogel & Reimers 1995) are based on total column densities due to the low resolution of the instruments used, so if we wish to compare our abundances to these studies (see §7), we should start with total column densities. The column densities integrated across the velocity range of the main low ion absorption (components 1 and 2) in this absorber are $\log N(\text{Si II}) = 13.28 \pm 0.12$, $\log N(\text{Al III}) = 12.31 \pm 0.10$, and $\log N(\text{Si IV}) = 13.95 \pm 0.05$. In this case, the H I column density appropriate for the model is the total, $\log N(\text{H I}) = 16.85$. With these column densities, we find that the photoionization model agrees with the measurements to within the 2σ uncertainties when $-0.62 \leq [\text{M}/\text{H}] \leq -0.43$.

Throughout the rest of this section we will use $[\text{M}/\text{H}] \approx -0.45$ as a rough estimate of the metallicity in this absorber since this value for $[\text{M}/\text{H}]$ provides the best fit to the component 1 column densities and agrees with the constraints set in the previous paragraph from the integrated column densities. How does the metallicity derived for this LL absorber compare to other intervening QSO absorption systems at similar redshifts? At first glance, $[\text{M}/\text{H}] \approx -0.45$ seems like a high metallicity for $z_{\text{abs}} = 2.315$. However, it may not be. Recently, several high quality abundance measurements for intervening damped Ly α QSO absorbers have appeared in the literature (Lu et al. 1996 and references therein, see their Table 16). In Figure 8 we show the Si and Al abundances measured in these damped Ly α absorbers with open circles. The filled triangles in Figure 8 indicate the *conservative* lower limits on $[\text{Si}/\text{H}]$ and $[\text{Al}/\text{H}]$ at $z_{\text{abs}} = 2.3150$ and 2.3155 from Table 4. We also show in Figure 8a the Si abundances derived by Steidel (1990) in a study of several high redshift LL absorbers (open squares). From this figure we see that the gas-phase Si and Al abundances in this LL absorber are comparable to the gas-phase abundances in a significant fraction of the damped Ly α absorbers at similar redshifts. The open star at $z = 0$ in Figure 8a is the diffuse cloud gas-phase abundance of Si observed in the Galactic halo (Savage & Sembach 1996). It is interesting to note that at $z_{\text{abs}} \approx 2$, $[\text{Si}/\text{H}]$ in many intervening QSO absorbers is already approaching the value observed in the gaseous halo of the Milky Way. It is also interesting to note that $[\text{Si}/\text{H}]$ appears to increase significantly when $z_{\text{abs}} \lesssim 3$. Lu et al. (1996) suggest that the sudden increase in metallicity at $z \approx 3$ is due to chemical enrichment from the first wide-spread star formation in high redshift galaxies. However the sample is small, and more abundance measurements are needed.

Some additional properties of this LL absorber can be derived from the models. Since we have assumed a value for the mean intensity at the Lyman limit $J_{\nu}(\text{LL})$, the hydrogen number

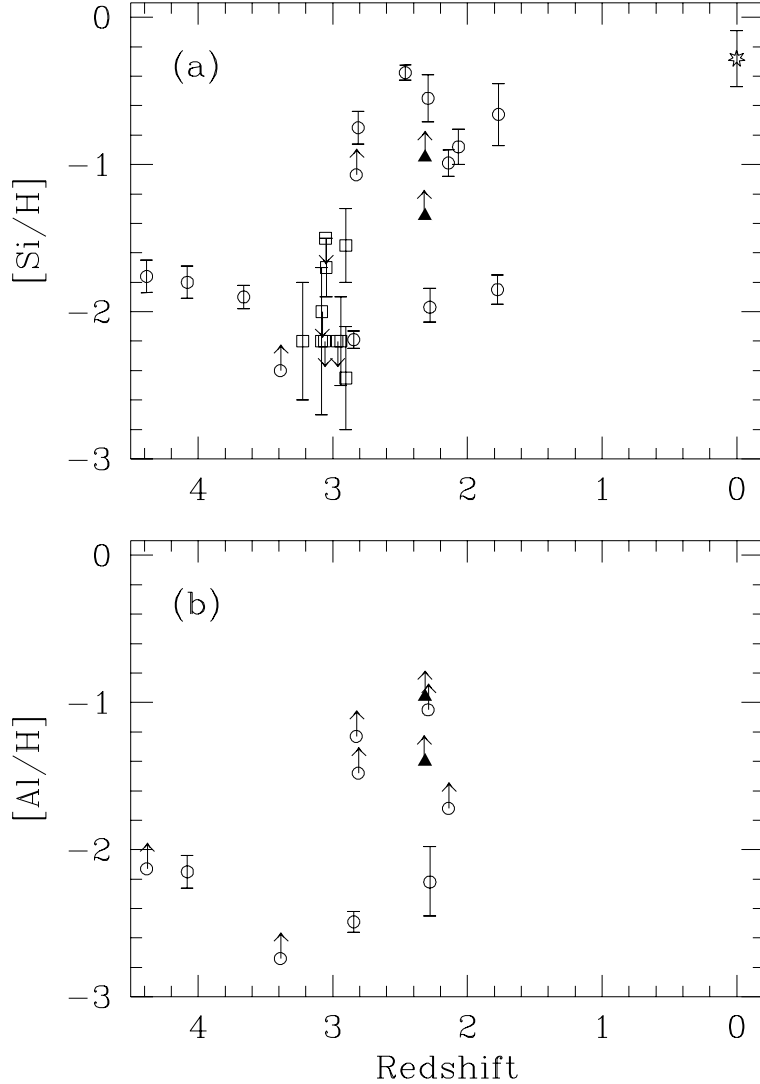


Fig. 8.— Metal abundances measured in damped Ly α QSO absorbers (open circles) as a function of redshift from Lu et al. (1996) and references therein for (a) silicon and (b) aluminum. In (a) we also show the abundances derived by Steidel (1990) for several high redshift Lyman limit absorbers (open squares). Limits are plotted with arrows. The conservative lower limits on [Si/H] and [Al/H] inferred in this paper for the Lyman limit absorber at $z_{\text{abs}} = 2.3150, 2.3155$ (see text §5.2.1) are indicated with filled triangles with arrows. Evidently, the silicon abundance in this LL absorber is comparable to the silicon abundance measured in several damped Ly α absorbers at similar redshifts. In panel (a), the open star at $z = 0$ shows the typical gas-phase abundance of Si observed in the Milky Way halo (Savage & Sembach 1996).

density can be determined from the ionization parameter. The top axis of Figure 6 indicates how n_{H} changes with Γ . The models also specify the thickness t of the absorber, and this in turn can be used to estimate the cloud mass, assuming the absorber is spherical (see §VIc in Steidel 1990). The model with $[\text{M}/\text{H}] = -0.45$ and $\log \Gamma = -2.6$ has $n_{\text{H}} = 0.02 \text{ cm}^{-3}$, $t = 240 \text{ pc}$, and cloud mass $M_{\text{c}} = 1.0 \times 10^5 M_{\odot}$. These rough estimates of t and M_{c} are close to the values predicted by the recent two-phase gaseous halo model of Mo & Miralda-Escudé (1996) for a cold photoionized phase embedded in a hot halo.

5.2.2. Other Lyman Limit Absorbers

We only detect C IV or Mg II absorption lines associated with the rest of the LL absorbers (see Table 2), so photoionization models cannot tightly constrain the elemental abundances (the level of ionization is unknown). Nevertheless, we can use CLOUDY models to place lower limits on the metallicities of these absorbers using equation 3 as discussed above. Applying this method with the Madau (1992) extragalactic radiation field, we derive $[\text{C}/\text{H}] \geq -2.26$ for the LL absorber at $z_{\text{abs}} = 1.84506$ and $[\text{C}/\text{H}] \geq -2.81$ for the LL absorber at $z_{\text{abs}} = 2.16797$. However, for the $z_{\text{abs}} = 1.84506$ system we also detect Mg II, and we derive a lower limit of $[\text{Mg}/\text{H}] \geq -0.45$. If we assume that the H I, Mg II, and C IV absorption lines at $z_{\text{abs}} = 1.84506$ all originate in the same gas, then the photoionization model requires $[\text{Mg}/\text{H}] = [\text{C}/\text{H}] = -0.43$. This must also be treated as a lower limit on $[\text{M}/\text{H}]$ since both Mg II and C IV are affected by absorption saturation at this redshift (see §4.5). Finally, applying this same method to the Mg II absorber at $z_{\text{abs}} = 1.15729$, we derive $[\text{Mg}/\text{H}] \geq -0.22$. Once again we see indications that high metallicities are already present in moderate redshift intervening absorbers.

5.2.3. Associated Absorber at $z_{\text{abs}} = 2.7125$

We detect C IV and rather strong N V absorption at $z_{\text{abs}} = 2.7125$ (lines 38-39 and 3-4 in Figure 1). We can also place good upper limits on the column densities of O I, C II, Al II, Si II, Fe II, and Si IV at this redshift since these lines are not in the Ly α forest. No absorption lines are apparent at the expected wavelengths; upper limits on these species along with the C IV and N V column densities are summarized in Table 5. The C IV and N V absorption lines are displaced by $\sim 600 \text{ km s}^{-1}$ from the emission redshift of the QSO and thus belong in the “associated” absorber class. Recent high resolution studies have shown that associated absorbers are often characterized by strong high ion absorption (especially N V) and overall metallicities comparable to or greater than solar (Wampler 1991; Petitjean et al. 1994; Savaglio et al. 1994; Hamann et al. 1995; Tripp et al. 1996; Hamann 1997). The ionization level of the HS 1700+6416 associated system inferred from the high ion column density ratios is similar to other associated absorbers and rather different from the ISM of the Milky Way. The $z_{\text{abs}} = 2.7125$ ionic ratios are $N(\text{C IV})/N(\text{N V}) < 0.2$ and $N(\text{C IV})/N(\text{Si IV}) > 5.2$, whereas Sembach et al. (1997) find that the median ratios in

the Galactic ISM are $N(\text{C IV})/N(\text{N V}) = 4.0 \pm 2.4$ and $N(\text{C IV})/N(\text{Si IV}) = 3.8 \pm 1.9$ based on 40 sight lines studied with *HST* and the *IUE*. For comparison, we note that Petitjean et al. (1994) report $N(\text{C IV})/N(\text{N V}) \sim 0.3$ and 0.4 for associated absorbers of PKS 0424-131 and Q 0450-131 respectively. This high degree of ionization is perhaps not surprising since associated absorbers are probably physically close to rather UV luminous QSOs, either somehow associated with the QSO nucleus/host galaxy or possibly occurring in the halos of galaxies in a cluster near the quasar, and the gas is predominantly photoionized by the QSO. Given the observed H I column density (see below), ionization corrections in the HS 1700+6416 associated system are certain to be large, so once again photoionization modeling is required to infer abundances.

In this associated absorber, we do not have the benefit of optically thin Lyman continuum absorption for the determination of $N(\text{H I})$, so we have used the H I Ly α absorption profile (the line at 4513.2 Å in Figure 1) to constrain the H I column density. Direct integration of the H I apparent column density profile at this redshift yields $\log N(\text{H I}) = 13.60 \pm 0.06$. For the purpose of this photoionization modeling effort, we assume that this H I column is not underestimated due to unresolved absorption saturation, but at any rate this provides a firm lower limit. If the H I absorption occurs in the same gas that produces the C IV and N V absorption (which is assumed when abundances are derived from a constant density single slab photoionized model), then at the likely gas temperatures the H I profile is well enough resolved so that any saturation should be apparent. Instead, the H I profile is broad and the apparent optical depth is only $\tau_a = 0.7$ in the deepest part of the profile. Furthermore, if this H I profile contains one or more components which are narrow enough to cause unresolved saturation, then these cold components might be detectable in low ionization stages such as C II, and they are not apparent (see Figure 1 and Table 5). Therefore, we shall proceed with the photoionization modeling using $\log N(\text{H I}) = 13.6$. However, we noted in §4.12 that the N V $N_a(v)$ profiles show evidence of unresolved saturation or incomplete covering of the QSO flux source. If the H I absorbing gas doesn't completely cover the QSO flux source, then the column density from direct integration of $N_a(v)$ may require a correction. This would increase the measured column density, and in the case of H I, this might decrease the metallicity required by the photoionization model to match the heavy element column densities. However, the heavy element column densities may be underestimated as well, so the corrections could push the model to higher or lower metallicities.

Since the QSO itself is likely to be the dominant source of ionization, we have used the observed spectral energy distribution (SED) of HS 1700+6416 for the input radiation field for CLOUDY abundance estimations. The QSO continuum is *detected* from $\lambda_r = 912$ Å (in the QSO frame) down to $\lambda_r \approx 320$ Å, which is the region of the spectrum which governs the ionization of most low and intermediate ionization stages and is close to the critical region of the spectrum where C III – C IV and N IV – N V are photoionized, i.e., $125 < \lambda_r < 300$ Å. However, since the observed QSO flux is attenuated by at least¹² seven optically thin Lyman limit absorbers

¹²The $z_{\text{abs}} = 0.72219$ absorber may be an eighth LL system with the Lyman continuum absorption undetected

Table 5. Associated System Column Densities

Species	Wavelength (\AA) ^a	$\log N$ (cm^{-2})
H I.....	1215.670	13.60 ± 0.06
O I.....	1302.168	$< 13.74^b$
C II.....	1334.532	$< 13.28^b$
Al II....	1670.787	$< 11.68^b$
Si II....	1526.707	$< 12.97^b$
Fe II....	1608.451	$< 13.21^b$
Si IV....	1393.755	$< 12.46^b$
C IV....	1548.195, 1550.770	13.18 ± 0.04
N V.....	1238.821, 1242.804	≥ 13.87

^aVacuum wavelength from Morton (1991).

^bColumn density upper limit derived from the 4σ upper limit on the rest equivalent width, assuming the linear part of the curve of growth applies.

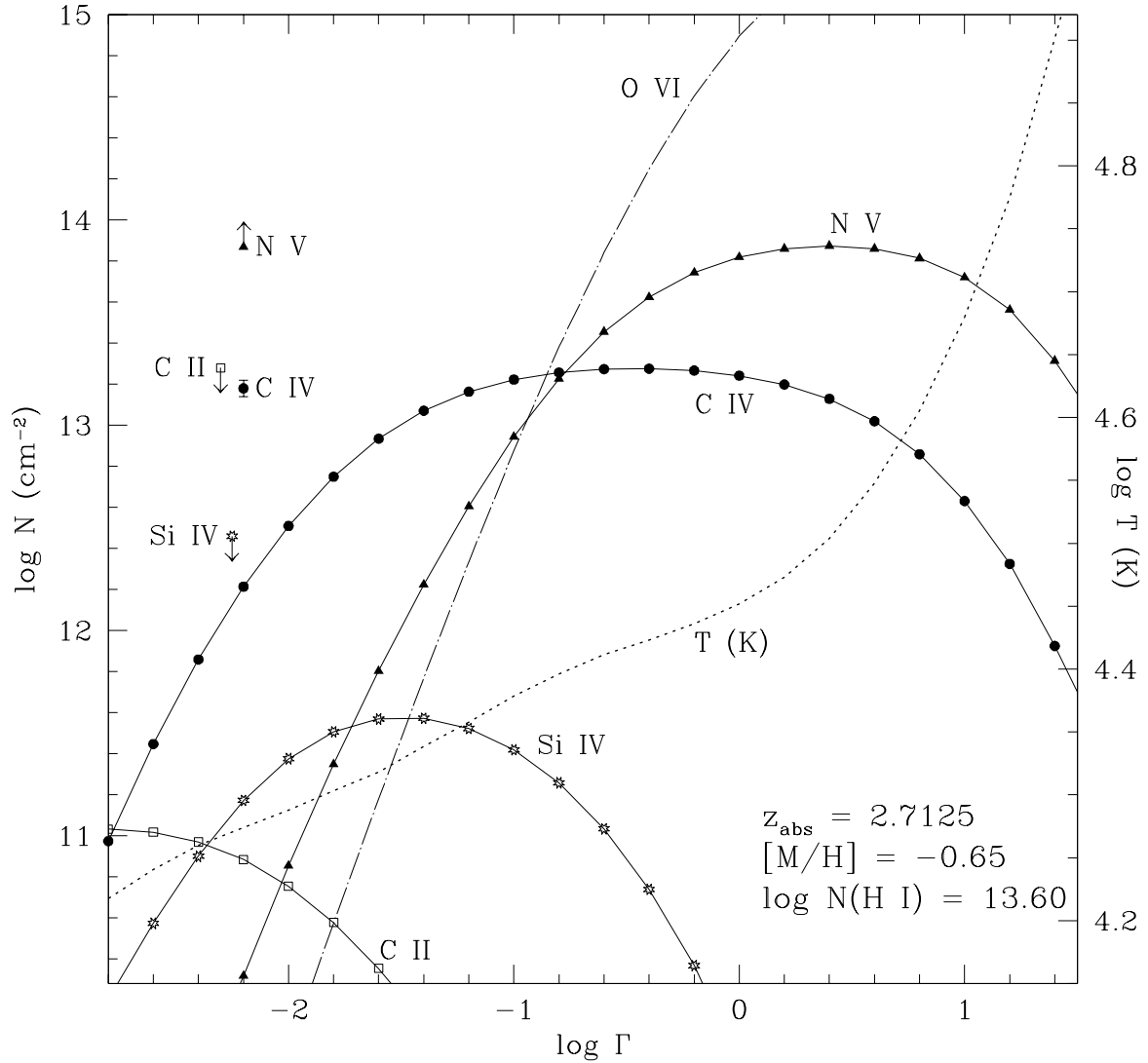


Fig. 9.— Column densities calculated by a photoionized model of the associated absorber of HS 1700+6416 at $z_{\text{abs}} = 2.7125$ (§5.2.3) as a function of ionization parameter Γ . The mean temperature of the model is plotted vs. Γ with a dotted line using the scale on the right axis. At the left side of the figure (arbitrarily placed near $\log \Gamma = -2.2$) the observed C IV column density (with 1σ error bars) and the limits on $N(\text{N V})$, $N(\text{Si IV})$ and $N(\text{C II})$ are indicated. The radiation field used for this calculation is the spectral energy distribution of the QSO assembled by Siemiginowska et al. (1996).

(see Figure 1 in Reimers et al. 1992), the true photoionizing flux impinging on the associated absorber gas is certainly greater than the observed flux. This true flux is difficult to estimate because the observed flux must be corrected for (1) the seven optically thin LL absorbers, (2) the net reddening introduced by any dust in intervening absorbers (which is smeared by the various redshifts of the intervening systems), and (3) attenuation by the Ly α forest and the ‘Ly α valley’, which includes the cumulative Lyman continuum absorption due to all of the intervening absorbers (Møller & Jakobsen 1990). The correction for the seven LL systems is straightforward (see equation 2), but we have little information on the magnitude and wavelength dependence of the other corrections. Several recent high resolution studies have suggested that there may be very little dust in intervening damped Ly α absorbers (Lu et al. 1995; Meyer, Lanzetta, & Wolfe 1995; Prochaska & Wolfe 1996; Lu et al. 1996). However, this conclusion has been contested by Pettini et al. (1997) who argue that the observed abundances are consistent with a modest amount of dust in the QSO absorbers. To derive a first-order estimation of the associated system metallicity, we have used the observed SED of HS 1700+6416 from Siemiginowska et al. (1996, see their Figure 2) for the CLOUDY radiation field. This SED is based on the *HST* FOS data from Reimers et al. (1992) combined with ground-based optical spectrophotometry, the ROSAT PSPC data from Reimers et al. (1995a), and an IRAS detection of the QSO at 60 μm . Siemiginowska et al. have corrected the *HST* UV spectrum for the seven LL absorbers, but they have not applied any corrections for intervening dust or Ly α forest/valley attenuation. Therefore the Siemiginowska et al. SED provides a firm lower limit on the photoionizing flux; various corrections could make the true flux greater, but the flux cannot be less than the Siemiginowska et al. SED.

We show in Figure 9 the column densities calculated by this model as a function of the ionization parameter Γ for $[\text{M}/\text{H}] = -0.65$ with solar relative abundances and $\log N(\text{H I}) = 13.6$. We show this particular model because it provides a lower limit on $[\text{N}/\text{H}]$ (see below). We also show in this figure how the mean temperature (dotted line) of the model changes with Γ , and we plot the observed C IV column density as well as the lower limit on $N(\text{N V})$ and the upper limits on $N(\text{C II})$ and $N(\text{Si IV})$ near (arbitrarily) $\log \Gamma = -2.2$. The constraints on the low ions and Si IV are easily satisfied by the model, and the model temperature is compatible with the upper limit set by the C IV line width (see Table 3). We see from Figure 9 that the model agrees with the observed C IV column density to within 2σ over a broad range in ionization parameter, $-1.4 \leq \log \Gamma \leq +0.4$. However, over most of this ionization parameter range, the model falls far short of the lower limit on $N(\text{N V})$. To produce enough N V, the model requires $\log \Gamma = +0.4$, and even then the model N V column is just barely large enough, which sets a lower limit of $[\text{N}/\text{H}] \geq -0.65$. For carbon the model requires $[\text{C}/\text{H}] \geq -0.82$. However, the true N V column density may be significantly larger than the lower limit in Table 5, and to obtain a higher N V/C IV ratio, Γ must be increased (see Figure 9). At higher values of Γ the C IV and N V column densities predicted by the model decrease, so the metallicity must in turn be increased as well to agree with

because it occurs in a region of the FOS spectrum with low S/N. The Mg II lines detected at this redshift are strong and saturated (see §4.1), so this absorber is likely to have an appreciable H I column.

the measured column densities. These limits assume solar N/C relative abundances. Hamann & Ferland (1993) have argued, on the basis of QSO *emission* line intensities, that nitrogen is overabundant relative to carbon in the immediate vicinity of a QSO. This may provide another means to boost the N V/C IV ratio in this associated absorber *if* the absorbing gas is close to the quasar, but in this case models with lower ionization parameters and lower metallicities can be brought into agreement with the measured column densities.

Associated system abundance measurements based on C IV and N V are sensitive to the shape of the ionizing continuum assumed for the model. Hamann (1997) has recently assembled a suite of photoionization models for the study of abundances in associated and broad absorption lines using a variety of continuum shapes, and we can use his work to illustrate this sensitivity to continuum shape. His continuum shape ‘A’ with a UV cutoff temperature $T_c = 10^{5.7}$ K (see Appendix in Hamann 1997) is consistent with the observed SED of HS 1700+6416 from Siemiginowska et al. (1996) in the FUV but has significantly higher flux in the ionizing ultraviolet where Siemiginowska et al. did not measure the QSO flux. Using this continuum shape ‘A’, we derive $[C/H] \geq -0.25$ and $[N/H] \geq +0.19$ for the associated system of HS 1700+6416. The continuum shape we used in the previous paragraph and in Figure 9 (based on Siemiginowska et al.) provides firm lower limits on $[C/H]$ and $[N/H]$ because this continuum is the lower limit on the ionizing flux. There are various corrections which could make the SED harder and hence increase the lower limits on $[C/H]$ and $[N/H]$.

Finally, we comment that these photoionization models are highly simplified, and there are some indications that the real absorbers are more complicated than the assumed models. Consider the Doppler parameters derived from profile fitting in Table 1. These b -values can be expressed as a sum with a term due to thermal motions (b_t) and a term which includes all non-thermal motions (b_{nt}) such as bulk motions and turbulence,

$$b^2 = b_{nt}^2 + b_t^2 = b_{nt}^2 + \frac{2kT}{m} = b_{nt}^2 + \frac{(0.129)^2 T}{A}, \quad (4)$$

where m is the mass and A is the atomic weight of the element and b is measured in km s^{-1} . For the photoionized models presented above, we assumed that all of the absorption lines of various species in a given component arise in a constant density gas slab. Therefore one might expect different elements to have the same values for b_{nt} and T , and higher mass elements should have lower b -values. In principle one can solve equation 4 for b_{nt} and T given b -values for two or more elements. However, in this associated absorber profile fitting yields $b = 25.2 \pm 1.3 \text{ km s}^{-1}$ for N V and $b = 11.4 \pm 1.1 \text{ km s}^{-1}$ for C IV. This is not consistent with the assumption that b_{nt} and T are the same for the C IV and N V absorption lines because this would require an unphysical negative temperature. This suggests that (1) there is some problem with the Doppler parameter measurements or uncertainties, or (2) the properties of the gas causing the C IV absorption are different from the properties of the gas producing the N V absorption. The disparity between $b(\text{N V})$ and $b(\text{C IV})$ cannot be blamed on the profile fitting procedure; attempts to fit the N V and C IV profiles with compatible b -values, assuming b_{nt} and T are the same, yield unacceptably

bad fits. The nitrogen line would be broader than the C IV line if N V is strongly saturated, but profile fitting should account for such saturation and yield consistent b -values. Therefore in this associated absorber, the C IV gas and N V gas do not have the same non-thermal motions and temperature. It is possible that the C IV absorption and *some* of the N V absorption occurs in the same gas cloud with additional N V absorption arising in a separate cloud which does not produce C IV absorption. Some support for this suggestion is provided by the fact that the N V profiles are affected by unresolved saturation and/or incomplete covering of the QSO flux source, while the C IV profiles show no evidence of these effects (see Figure 5). Future studies of this type of QSO absorber may require more intricate models.

6. Weak Mg II Systems

Based on a survey of Mg II absorption lines in the spectra of 103 QSOs, Steidel & Sargent (1992) conclude that there is paucity of *weak* Mg II lines, and they assert that “at least 80% of the Mg II absorbers are accounted for in a sample sensitive to $W_r^{\min} = 0.3 \text{ \AA}$ ” (W_r^{\min} is the minimum rest equivalent width in the sample). We draw a different (albeit tentative) conclusion from our high resolution high S/N spectra of HS 1700+6416 and HS 1946+7658 (Tripp et al. 1996). The sensitivity of our spectra of these QSOs is adequate for detection of Mg II lines with restframe equivalent width W_r as small as 0.03 \AA (at the 4σ level) over a total redshift path $\Delta z = 2.56$. We detect six definite Mg II absorbers in the spectra of these QSOs, and only one of these Mg II lines has $W_r \geq 0.3\text{\AA}$. To expand the sample size, we can combine our data with the similar quality spectra of PKS 0424–131 ($z_{\text{em}} = 2.1657$) and Q 0450–131 ($z_{\text{em}} = 2.2535$) obtained by Petitjean et al. (1994)¹³. From this combined sample of four quasars, we derive a mean number of Mg II absorbers per unit redshift of $dN/dz = 2.3 \pm 0.8$. From their sample of Mg II absorbers with $W_r \geq 0.3\text{\AA}$, Steidel & Sargent (1992) derive $dN/dz = 0.97 \pm 0.10$. It is important to emphasize that dN/dz derived from our sample of four quasars is highly uncertain due to the small sample. However, Womble (1995) has recently detected a similar excess of *weak* Mg II systems ($W_r \geq 0.015 \text{ \AA}$) in a high S/N high resolution Keck spectrum of PG 1634+706 ($z_{\text{em}} = 1.334$). Furthermore, Steidel & Sargent find that dN/dz increases smoothly as the minimum W_r in the sample decreases from 1.0 \AA to 0.3 \AA (see their Figure 5). This also suggests that dN/dz is dominated by weak Mg II systems. This excess of weak Mg II lines may indicate that the cross section of the Mg II absorbers is large; Womble estimates that the required radius is $\sim 90 h^{-1} \text{ kpc}$ ($h = H_0/100 \text{ km s}^{-1} \text{ Mpc}^{-1}$) for lines with $W_r \geq 0.015 \text{ \AA}$. An excess of weak Mg II absorbers may also have implications for the study of galaxies *selected* because they produce Mg II absorption in the spectrum of the background QSO. For example, Steidel, Dickinson, & Persson (1994) find that their sample of Mg II absorbers are mostly associated with normal luminous galaxies, but their

¹³The spectra obtained by Petitjean et al. (1994) have a resolution of $\sim 20 \text{ km s}^{-1}$ and sufficient S/N for detection of all lines with $W_r \geq 0.03\text{\AA}$.

sample may be biased against underluminous galaxies because of the lower equivalent width cutoff (they select Mg II systems with $W_r \geq 0.3 \text{ \AA}$ for follow-up imaging and redshift measurements). With the echelle spectrograph on the Keck telescope, it should be straightforward to confirm or refute this excess of weak Mg II absorbers with a larger sample.

As discussed by Petitjean & Bergeron (1990) and Steidel & Sargent (1992), there are some indications that the fractions of Mg II absorbers which are weak and strong may evolve with redshift in the sense that there are more strong Mg II lines at higher redshift. This probably is not the reason that the dN/dz obtained by Steidel & Sargent is lower than the dN/dz we have derived because the redshift range probed by Steidel & Sargent, $0.2 \leq z_{\text{abs}} \leq 2.2$, is similar to the redshift range probed by our sample, $0.4 \leq z_{\text{abs}} \leq 2.1$.

7. Comments on *HST* FOS Abundances

The *HST* FOS observation of HS 1700+6416 obtained by Reimers et al. (1992) is groundbreaking work, and the spectrum has provided an excellent reconnaissance of this extraordinary sight line. However, the data have some serious limitations due to the low resolution (FWHM $\sim 300 \text{ km s}^{-1}$) of the FOS, and we suspect that the abundances derived from the FOS data by Vogel & Reimers (1995) are unreliable. Several problems are introduced by the low resolution of the data combined with the high redshift of the QSO (which leads to a very high line density in the FOS spectral region including metal lines, He lines, and many H I Lyman series lines): (1) In many cases, the absorption lines are strongly blended with several lines of different species at different redshifts (see Figure 4 in Vogel & Reimers 1995), and extracting accurate column densities from the blends is rather difficult. (2) As Lipman, Pettini, & Hunstead (1995) have noted (see their Figure 1), narrow lines are unlikely to be detected in the FOS spectrum, and the FOS line list will be biased toward strongly saturated lines which do not provide reliable column densities. (3) Quasar absorption line profiles frequently show multiple components which will be completely unresolved at the FOS resolution, and consequently absorption by low and high ionization species which appear to be at the same redshift in the FOS data may not actually be associated (i.e., the low and high ion absorption occur in different unresolved components). Confusion due to multiple unresolved components will be especially severe in the absorption line complex at $2.432 < z_{\text{abs}} < 2.441$ (see §4.10).

This paper confirms that the Vogel & Reimers (1995) abundances may be problematic. For example, we estimate that the strongest component of the LL absorber at $z_{\text{abs}} = 2.3150$ has $[\text{Si}/\text{H}] \geq -0.95$ and $[\text{Al}/\text{H}] \geq -0.96$ and is best fit with $[\text{M}/\text{H}] \approx -0.45$ (see §5.2.1), while Vogel & Reimers report $[\text{N}/\text{H}] < -1.04$ and $[\text{O}/\text{H}] = -1.52$. The low resolution of the FOS also yields redshifts which may not be accurate enough to facilitate line identifications. Consider the LL system for which Vogel & Reimers give $z_{\text{abs}} = 1.8465$. We detect the Mg II doublet at high significance levels at $z_{\text{abs}} = 1.84506$ (lines 44 and 45 in Figure 1), which differs from the Vogel & Reimers redshift by $\sim 150 \text{ km s}^{-1}$. This amount of uncertainty in z can make line identification difficult given

the high density of lines, and indeed Petitjean et al. (1996) have pointed out several lines that Vogel & Reimers may have incorrectly identified because they were not aware of the associated absorption system of HS 1700+6416. Similarly, the extended X-ray sources near the sight line (see §1) may produce absorption lines, at $z_{\text{abs}} = 0.225$ in the case of Abell 2246, and these low redshift absorption lines could have been misidentified as well. These problems are generic drawbacks of low resolution data which should be greatly alleviated when HS 1700+6416 is observed with the Space Telescope Imaging Spectrograph.

8. Summary

The paper is summarized as follows.

(1) We have obtained a high S/N high resolution (20 km s^{-1} FWHM) spectrum of HS 1700+6416 ($z_{\text{em}} = 2.72$) with complete spectral coverage from 4300 to 8350 Å. Thirteen absorption systems with metals are detected in this optical spectrum, including six absorbers which cause optically thin Lyman limit absorption in the *HST* spectrum obtained by Reimers et al. (1992).

(2) Four C IV doublets are narrow ($b < 8 \text{ km s}^{-1}$) which indicates that these absorbers are relatively cool ($T < 50000 \text{ K}$) and probably photoionized.

(3) A dense cluster of C IV doublets is detected at $2.432 < z_{\text{abs}} < 2.441$, which corresponds to a displacement of $\sim 24000 \text{ km s}^{-1}$ from the QSO emission redshift. Despite the large displacement from z_{em} , two pairs of C IV doublets are apparently line locked, i.e., the strong line of one C IV absorber is aligned with the weak line of a different C IV doublet, to within 10 km s^{-1} in one case and to within 25 km s^{-1} in the other case. This may be the remnant (or precursor) of a BAL outflow. However, it is possible that these alignments are coincidental rather than true line locking.

(4) The column density ratios of high ionization stages in the Lyman limit absorber at $z_{\text{abs}} = 2.3150$ differ significantly from the ratios observed in the gaseous halo of the Milky Way. For example, $N(\text{C IV})/N(\text{Si IV}) \geq 10$ in two components of this absorber. This high ionic ratio in the LL absorber is not expected in cooling galactic fountain gas but could be produced in supernova remnants, conductive interfaces between warm and hot gas, turbulent mixing layers, or from photoionization by the diffuse extragalactic background radiation.

(5) Photoionization modeling of the Lyman limit absorber at $z_{\text{abs}} = 2.3150$ places conservative lower limits on $[\text{Si}/\text{H}]$ and $[\text{Al}/\text{H}]$. The model which provides the best fit has $[\text{M}/\text{H}] \approx -0.45$. This is substantially larger than the metallicity derived by Vogel & Reimers (1995) from the *HST* FOS spectrum. The discrepancy is probably due to the low resolution of the FOS data which causes severe blending and saturation problems.

(6) An associated absorber at $z_{\text{abs}} = 2.7125$ shows C IV and strong N V lines. The C IV lines are unsaturated, but the N V apparent column density profiles indicate that N V is affected by

unresolved saturation, or the N V absorbing gas does not completely cover the QSO flux source.

(7) Despite coverage of several low ionization stages of abundant elements with high $f\lambda$ values, no low ion absorption is evident in the associated absorber. Also, the high ion column density ratios differ significantly from the ratios observed in the Milky Way ISM. This indicates that the absorber is highly ionized, presumably by the QSO. Photoionization modeling using the QSO spectral energy distribution for the input radiation field requires $[N/H] \geq -0.65$ and $[C/H] \geq -0.82$. These are firm lower limits which could be increased by plausible corrections to the ionizing continuum shape. However, profile fitting yields $b(N\text{ V}) = 25.2 \pm 1.3 \text{ km s}^{-1}$ and $b(C\text{ IV}) = 11.4 \pm 1.1$, and therefore the gas which produces the N V absorption does not have the same temperature and/or non-thermal motions as the C IV gas, and a more complex photoionization model may be required for this absorber.

(8) We briefly examine the number of Mg II absorbers detected per unit redshift. The line density appears to be dominated by weak Mg II lines with $W_r < 0.3 \text{ \AA}$, but the sample suffers from small number statistics.

It is a pleasure to thank Fred Hamann for several excellent comments which significantly improved this paper. We acknowledge Gary Ferland for use of his photoionization code CLOUDY, and we thank Ken Lanzetta for sharing software which was used for profile fitting. Kathy Romer and David Cohen provided helpful comments on the ROSAT data and the nature of the extended X-ray sources near HS 1700+6416. T.M.T. received support from NASA grant NGT51003. This research is also supported by NASA through grant HF1062.01-94A for L.L. from the Space Telescope Science Institute, which is operated by the Association of Universities for Research in Astronomy, Inc., for NASA under contract NAS5-26555. B.D.S. acknowledges support from NASA grant NAG5-1852.

REFERENCES

- Arav, N., Korista, K. T., Barlow, T. A., & Begelman, M. C. 1995, *Nature*, 376, 576
- Arav, N., Li, Z.-Y., & Begelman, M. C. 1994, *ApJ*, 432, 62
- Barlow, T. A., & Sargent, W. L. W. 1997, *AJ*, 113, 136
- Beaver, E. A., et al. 1991, *ApJ*, 377, L1
- Bechtold, J. 1995 in *QSO Absorption Lines*, ed. G. Meylan, (Berlin:Springer), 299
- Benjamin, R. A., & Shapiro, P. R. 1997, *ApJS*, submitted
- Bergeron, J., & Stasińska, G. 1986, *A&A*, 169, 1
- Cowie, L. L., Songaila, A., Kim, T.-S., & Hu, E. M. 1995, *AJ*, 109, 1522
- Edgar, R. J., & Chevalier, R. A. 1986, *ApJ*, 310, L27

- Ferland, G. J. 1993, University of Kentucky Department of Physics and Astronomy Internal Report
- Foltz, C. B., Chaffee, F. H., Weymann, R. J., & Anderson, S. F. 1988, in *Quasar Absorption Lines: Probing the Universe*, ed. J. C. Blades, D. A. Turnshek, & C. A. Norman (Cambridge: Cambridge University Press), 53
- Foltz, C. B., Weymann, R. J., Morris, S. L., & Turnshek, D. A. 1987, *ApJ*, 317, 450
- Grevesse, N., & Anders, E. 1989, in *Cosmic Abundances of Matter*, ed. C. J. Waddington, (New York: American Institute of Physics), 1
- Hamann, F. 1997, *ApJS*, in press
- Hamann, F., Barlow, T. A., Beaver, E. A., Burbidge, E. M., Cohen, R. D., Junkkarinen, V., & Lyons, R. 1995, *ApJ*, 443, 606
- Hamann, F., Barlow, T. A., & Junkkarinen, V. 1997a, *ApJ*, in press
- Hamann, F., Barlow, T. A., Junkkarinen, V., & Burbidge, E. M. 1997b, *ApJ*, in press
- Hamann, F., & Ferland, G. 1993, *ApJ*, 418, 11
- Horne, K. 1986, *PASP*, 98, 609
- Jakobsen, P., Boksenberg, A., Deharveng, J. M., Greenfield, P., Jedrzejewski, R., & Paresce, F. 1994, *Nature*, 370, 35
- Jannuzi, B. T., et al. 1996, *ApJ*, 470, L11
- Jenkins, E. B. 1987, in *Interstellar Processes*, ed. D. J. Hollenbach & H. A. Thronson (Dordrecht: Reidel), 533
- Jenkins, E. B. 1996, *ApJ*, 471, 292
- Lanzetta, K. M., & Bowen, D. V. 1992, *ApJ*, 391, 48
- Lipman, K., Pettini, M., & Hunstead, R. W. 1995, in *QSO Absorption Lines*, ed. G. Meylan, (Berlin:Springer), 89
- Lockman, F. J., & Savage, B. D. 1995, *ApJS*, 97, 1
- Lyons, R. W., Cohen, R. D., Junkkarinen, V. T., Burbidge, E. M., & Beaver, E. A. 1995, *AJ*, 110, 1544
- Lu, L., Sargent, W. L. W., & Barlow, T. A., Churchill, C. W., & Vogt, S. 1996, *ApJS*, 107, 475
- Lu, L., Savage, B. D., Tripp, T. M., & Meyer, D. M. 1995, *ApJ*, 447, 597
- Madau, P. 1992, *ApJ*, 389, L1
- McWilliam, A., Preston, G., Sneden, C., & Searle, L. 1995, *AJ*, 109, 2757
- Meyer, D. M., Lanzetta, K. M., & Wolfe, A. M. 1995, *ApJ*, 451, L13
- Mo, H. J., & Miralda-Escudé, J. 1996, *ApJ*, 469, 589
- Møller, P., & Jakobsen, P. 1990, *A&A*, 228, 299

- Morris, S. L., Weymann, R. J., Foltz, C. B., Turnshek, D. A., Shectman, S., Price, C., & Boroson, T. A. 1986, *ApJ*, 310, 40
- Morton, D. C. 1991, *ApJS*, 77, 119
- Murray, N., Chaing, J., Grossman, S. A., & Voit, G. M. 1995, *ApJ*, 451, 498
- Perry, J. J., Burbidge, E. M., & Burbidge, G. R. 1978, *PASP*, 90, 337
- Petitjean, P., & Bergeron, J. 1990, 231, 309
- Petitjean, P., Rauch, M., & Carswell, R. F., 1994, *A&A*, 291, 29
- Petitjean, P., Riediger, R., & Rauch, M. 1996, *A&A*, 307, 417
- Pettini, M., King, D. L., Smith, L. J., & Hunstead, R. W. 1997, *ApJ*, submitted
- Pettini, M., Smith, L. J., Hunstead, R. W., & King, D. L. 1994, *ApJ*, 426, 79
- Picard, A., & Jakobsen, P. 1993, *A&A*, 276, 331
- Prochaska, J. X., & Wolfe, A. M. 1996, *ApJ*, 470, 474, 140
- Rauch, M., Sargent, W. L. W., Womble, D. S., & Barlow, T. A. 1996, *ApJ*, 467, L5
- Reimers, D., Bade, N., Schartel, N., Hagen, H.-J., Engels, D., & Toussaint, F. 1995a, *A&A*, 296, L49
- Reimers, D., Clavel, J., Groote, D., Engels, H. J., Naylor, T., Wamsteker, W., & Hopp, U. 1989, *A&A*, 218, 71
- Reimers, D., Rodríguez-Pascual, P., Hagen, H.-J., & Wisotzki, L. 1995b, *A&A*, 293, L21
- Reimers, D., Vogel, S., Hagen, H.-J., Engels, D., Groote, D., Wamsteker, W., Clavel, J., & Rosa, M. R. 1992, *Nature*, 360, 561
- Robertson, J. G. 1986, *PASP*, 98, 1220
- Rodríguez-Pascual, P. M., de la Fuente, A., Sanz, J. L., Recondo, M. C., Clavel, J., Santos-Lleó, M., & Wamsteker, W. 1995, *ApJ*, 448, 575
- Romer, A. K. 1996a, private communication
- Romer, A. K., Ulmer, M. P., Nichol, B. C., Holden, B. P., Burke, D., & Collins, C. A. 1996b, *BAAS*, 28, 853
- Ryan, S. G., Norris, J. E., & Beers, T. C. 1996, *ApJ*, 471, 254
- Sanz, J. L., Clavel, J., Naylor, T., & Wamsteker, W. 1993, *MNRAS*, 260, 468
- Sargent, W. L. W., Boksenberg, A., & Steidel, C. C. 1988, *ApJS*, 68, 539
- Savage, B. D., & Sembach, K. R. 1991, *ApJ*, 379, 245
- Savage, B. D., & Sembach, K. R. 1996, *ARA&A*, 34, 279
- Savaglio, S., D’Odorico, S., & Møller, P. 1994, *A&A*, 281, 331
- Scoville, N., & Norman, C. 1995, *ApJ*, 451, 510

- Sembach, K. R., & Savage, B. D. 1992, *ApJS*, 83, 147
- Sembach, K. R., Savage, B. D., & Tripp, T. M. 1997, *ApJ*, in press
- Siemiginowska, A., Bechtold, J., Tran, K.-V., & Dobrzycki, A. 1996, in *Science with the Hubble Space Telescope - II*, ed. P. Benvenuti, F. D. Macchetto, & E. J. Schreier, STScI/ST-ECF Workshop, 181
- Sofia, U. J., Cardelli, J. A., & Savage, B. D. 1994, *ApJ*, 430, 650
- Spitzer, L. 1978, *Physical Processes in the Interstellar Medium*, (New York: John Wiley & Sons)
- Steidel, C. C., 1990, *ApJS*, 74, 37
- Steidel, C. C., Dickinson, M., & Persson, S. E. 1994, *ApJ*, 437, L75
- Steidel, C. C., & Sargent, W. L. W. 1989, *ApJ*, 343, L33
- Steidel, C. C., & Sargent, W. L. W. 1992, *ApJS*, 80, 1
- Sutherland, R. S., & Dopita, M. A. 1993, *ApJS*, 88, 253
- Tripp, T. M., Bechtold, J., & Green, R. F. 1994, *ApJ*, 433, 533
- Tripp, T. M., Lu, L., & Savage, B. D. 1996, *ApJS*, 102, 239
- Turnshek, D. A. 1988 in *Quasar Absorption Lines: Probing the Universe*, ed. J. C. Blades, D. A. Turnshek, & C. A. Norman (Cambridge: Cambridge University Press), 17
- Turnshek, D. A., Weymann, R. J., & Williams, R. E. 1979, *ApJ*, 230, 330
- Tytler, D., Fan, X.-M., Burles, S., Cottrell, L., Davis, C., Kirkman, D., & Zuo, L. 1995, in *QSO Absorption Lines*, ed. G. Meylan, (Berlin:Springer), 289
- Verner, D. A., Tytler, D., & Barthel, P. D. 1994, *ApJ*, 430, 186
- Viegas, S. M. 1995, *MNRAS*, 276, 268
- Vogel, S., & Reimers, D. 1995, *A&A*, 294, 377
- Wampler, E. J. 1991, 368, 40
- Wampler, E. J., Bergeron, J., & Petitjean, P. 1993, *A&A*, 273, 15
- Weymann, R. J., Carswell, R. F., & Smith, M. G. 1981, *ARA&A*, 19, 41
- Wheeler, J. C., Sneden, C., & Truran, J. W. 1989, *ARA&A*, 27, 279
- Womble, D. S. 1995 in *ESO Workshop on QSO Absorption Lines*, ed. G. Meylan, (Berlin: Springer), 157